Masters Program in **Geospatial Technologies**

Detection of Artisanal Small-Scale Mining(ASM) Using Segmentation-Based Deep Learning and Sentinel 2 Imagery In Madre de Dios, Peru.

Augustine Ofobi Aborah

Dissertation submitted in partial fulfilment of the requirements for the Degree of *Master of Science in Geospatial Technologies*

NOVA IMS Information Management School · Universitat Jaume I · Universität Münster

Universität Münster, Germany

Institute for Geoinformatics

Detection of Artisanal Small-Scale Mining(ASM) Using Segmentation-Based Deep Learning and Sentinel 2 Imagery In Madre de Dios, Peru.

by

Augustine Ofobi Aborah

Master Dissertation presented as partial requirement for obtaining the Master's Degree in Geospatial Technologies

Supervised by

Mana Gharun, PhD,

University of Münster

Münster, Germany

Co-supervised by

Marco Octávio Trindade Painho, PhD,

NOVA Information Management School

Lisboa, Portugal

&

Filiberto Pla, PhD,

Universitat Jaume I

Castellón, Spain

20th February, 2026

STATEMENT OF INTEGRITY

I declare that the work described in this document is my own and not from someone else. All the assistance I have received from other people is duly acknowledged and all the sources (published or not published) are referenced.
This work has not been previously evaluated or submitted to the University of Münster or elsewhere. I further declare that I have fully acknowledged the Rules of Conduct and Code of Honor from the University of Münster.

Münster, 20th February, 2026.

____

Augustine Ofobi Aborah.

USE OF GENERATIVE ARTIFICIAL INTELLIGENCE

Tasks	NO	YES	Generative Artificial Intelligence tools
Better understand issues related to the research		X	Perplexity, ChatGPT
Summarizing text from bibliography / resources	X		
Summarizing the method(s) used		X	ChatGPT
Translating text	X		
Grammar check		X	ChatGPT
Paraphrase or rewriting text from other people / resources	X		
Coding in R, Python, etc.		X	ChatGPT
Get help on a software		X	ChatGPT
Creating and editing images, maps, videos, etc.	X		
Data analysis	X		
Specify below other tasks not mentioned above:			

DEDICATION

This thesis is dedicated to Mr. Joseph Kwame Aborah and Mrs. Comfort Antwi, whose unwavering support, encouragement, and sacrifices have been the foundation of my academic journey. Your silent prayers and steadfast belief in me have continually inspired me to persevere through every challenge.

ACKNOWLEDGMENTS

I am deeply thankful to my family for their continuous support, encouragement, and unwavering belief in me throughout this journey. Your strength and confidence in me have been a constant source of motivation.

I would also like to express my sincere gratitude to my supervisors; Professor Mana Gharun, Professor Marco Octávio Trindade Painho, and Professor Filiberto Pla for their patience, invaluable guidance, and constructive feedback throughout this research. Your insight, dedication, and academic mentorship have significantly shaped the direction of this work and strengthened my interest in research.

Finally, I am grateful to my colleagues for their support, thoughtful discussions, and the ideas they generously shared. To everyone who contributed in any capacity to the completion of this research, I extend my heartfelt appreciation and a very big thank you.

ABSTRACT

Artisanal and small-scale mining (ASM) is a major driver of environmental degradation in tropical regions, contributing to deforestation, land degradation, and water pollution. However, mapping ASM activities using satellite imagery remains challenging due to their small spatial extent, spectral variability, and similarity to other forms of land disturbance. This study aims to investigate how transferable ASM models can be from one mining site to another and focuses on two major ASM hotspots: Madre de Dios, Peru (source region), and the Kayapó Indigenous Territory, Brazil (target region), with analysis conducted using multi-temporal Sentinel-2 imagery acquired between January to July of 2024. The study presents a deep learning–based approach for detecting ASM sites using multi-temporal Sentinel-2 imagery and forest loss information derived from the Hansen Global Forest Change dataset. A U-Net semantic segmentation model with a ResNet50 encoder was employed to capture both fine-scale spatial details and high-level contextual features associated with mining activities.

The model was trained using labeled data generated from areas of forest disturbance and evaluated using standard segmentation metrics, including Intersection over Union (IoU), Dice coefficient, precision, recall, and F1-score. Within the source region (Madre de Dios), the best-performing model achieved an F1-score of 0.933 and an IoU of 0.880, with overall accuracy ranging between 0.96 and 0.97 across feature configurations. To assess model generalization, both zero-shot transfer and fine-tuning experiments were conducted across geographically distinct regions characterized by differences in vegetation structure, soil properties, and mining morphology. Direct zero-shot transfer to Kayapó resulted in a reduced F1-score of 0.763 and an IoU of 0.648, reflecting substantial performance degradation due to domain shift. However, transfer learning through limited fine-tuning improved performance to an F1-score of 0.850 and an IoU of 0.749, increasing spatial overlap with reference ASM areas from 51.66% to 80.06%.

Spatial overlap analysis further demonstrated the model's ability to capture mining-related land cover changes beyond conventional forest loss mapping, highlighting its potential as a complementary tool for environmental monitoring. Despite limitations associated with the use of global forest loss data as proxy ground truth, the study

demonstrates that deep learning combined with freely available satellite imagery offers a scalable framework for ASM detection. The findings contribute to the development of transferable remote sensing models for monitoring environmentally destructive activities in data-scarce regions.

KEYWORDS

Artisanal Small-Scale Mining; Deep Learning; Remote Sensing; Transfer Learning

Sustainable Development Goals (SGD):

[select ONLY the correspondent SGDs according to this Master Thesis Contribution(s) https://sdgs.un.org/goals, and delete the remaining images]

Table of Content

INDEX OF TABLES

INDEX OF FIGURES

ACRONYMS

ASM – Artisanal Small Scale Mining

ASGM – Artisanal Small Scale Gold Mining

DL – Deep Learning

RS – Remote Sensing

CNN – Convolution Neural Network

NIR – Near Infrared

SWIR – Short Wave Infrared

NDVI – Normalized Difference Vegetation Index

EVI – Enhanced Vegetation Index

MNDWI – Modified Normalized Difference Water Index

SSCs – Suspended Sediment Concentrations

KIL – Kayapó Indigenous Land

SMP – Segmentation Models Pytorch

TL – Transfer Learning

1. INTRODUCTION

1.1 Problem Statement

Artisanal and Small-Scale Mining (ASM) constitutes a major source of livelihood for millions of people across the Global South, especially in rural and economically marginalized regions (Ofori-Ampofo et al., 2025; Seccatore et al., 2014). Despite its socioeconomic importance, ASM is frequently associated with severe environmental degradation, public health risks, and social challenges, including deforestation, water pollution, mercury contamination, and unsafe working conditions (Asner et al., 2013; Basu et al., 2015; Fritz et al., 2014; Gallwey et al., 2020; Gerson et al., 2022). The clandestine nature of many ASM operations, together with weak regulatory oversight and limited technical capacity, further increases these impacts, making effective governance and monitoring of ASM activities an urgent priority (Asner et al., 2013; Becerra et al., 2024; IUCN NL, 2024).

Madre de Dios, located in the southeastern Peruvian Amazon, has become the epicenter of illegal mining activities, leading to the destruction of forests and the degradation of vital ecosystems (Asner et al., 2013; Gallwey et al., 2020; Kopec et al., 2025; USAID, 2020). This region has experienced extensive deforestation driven by artisanal small-scale gold mining (ASGM), with nearly 500 km² of forest loss recorded between 1999 and 2012 alone (Diringer et al., 2020; Swenson et al., 2011). The expansion of ASM in Madre de Dios has been accelerated by rising gold prices following the 2008 global financial crisis and by increased accessibility resulting from the completion of the Interoceanic Highway which opened previously remote forest areas to mining activities (Asner et al., 2010; Asner & Tupayachi, 2016; Caballero Espejo et al., 2018; Nicolau et al., 2019; Saka et al., 2024). In addition to deforestation, ASM in the region has contributed to widespread mercury pollution, ecosystem degradation, and elevated risks to human health, particularly through contamination of soils, surface waters, and aquatic food chains (Diringer et al., 2015, 2020).

Effective monitoring of ASM remains a major challenge due to the extensive spatial extent of mining landscapes, terrain, limited accessibility, and persistent security concerns that restrict field-based data collection (Nava et al., 2022; Pasanisi et al., 2025). As a result, satellite-based remote sensing (RS) has emerged as a key tool for monitoring and mapping large-scale environmental changes including ASM activities (Peña-Villacreses et al., 2024). Among the various RS tools, Sentinel-2 imagery, which offers multispectral data at high spatial and temporal resolutions, has proven to be highly effective in detecting land cover changes caused by mining activities (Fonseca et al., 2024). ASM features observable from space are mostly surface-based and alluvial in nature, often appearing as clustered excavation pits, mining ponds, and exposed sediment deposits located along river networks (Owusu-Nimo et al., 2018; Snapir et al., 2017). However, these features can exhibit strong spectral and spatial similarities to other land-cover types such as water bodies, sand-mined areas, or urban settlements, complicating accurate discrimination using conventional mapping approaches (Ofori-Ampofo et al., 2025).

Traditional land use and land cover (LULC) mapping methods for ASM detection have largely relied on pixel-based classification using spectral information and conventional machine learning algorithms. While these approaches have enabled rapid regional-scale mapping, they often struggle to capture the complex spatial patterns and contextual information required to accurately delineate ASM features, particularly in heterogeneous tropical environments (Gallwey et al., 2020). Furthermore, the scarcity of publicly available ASM reference datasets and often inaccessible nature of mining areas for field surveys limits reproducibility and constrains the broader operational use of existing models by researchers and decision-makers (Ofori-Ampofo et al., 2025; USAID, 2020).

Recent advances in deep learning (DL), particularly convolutional neural network (CNN)-based semantic segmentation models such as U-Net, have demonstrated improved performance in RS applications by enabling pixel-level delineation of complex land-cover features while incorporating spatial context (Camalan et al., 2022; Jiang et al., 2024). Several studies have successfully applied U-Net architectures with Sentinel-2 imagery to map ASM and associated environmental changes in different geographic contexts, highlighting the potential of segmentation-based approaches for ASM monitoring (Gallwey et al., 2020; Nava et al., 2022). Despite these advances, DL applications for ASM detection remain at an early stage, and significant methodological challenges persist.

In particular, the transferability and generalization of segmentation-based ASM detection models across different geographic regions have not been systematically addressed. Variations in environmental conditions, mining practices, landscape structure, and spectral characteristics between regions such as Madre de Dios and the Kayapó

Indigenous Territory in Brazil may result in performance degradation when models are applied beyond their training domain (Ofori-Ampofo et al., 2025). This thesis therefore seeks to evaluate the effectiveness of segmentation-based DL models for ASM detection in Madre de Dios using Sentinel-2 imagery and to investigate the transferability and performance benefits of transfer learning (TL) when applying these models to a different geographical area, in this study, Kayapó, Brazil.

1.2 BACKGROUND

It is estimated that more than 40 million individuals are directly engaged in ASM activities worldwide with an additional 150 million people indirectly dependent on the sector for income and subsistence (Fritz et al., 2014; USAID, 2020). Unlike large-scale mining operations, ASM is typically characterized by small production units, informal or weakly enforced regulatory frameworks, and labor-intensive extraction methods. These characteristics shape the socioeconomic dynamics of mining communities while simultaneously increasing the vulnerability of local environments and populations to negative impacts (Ofori-Ampofo et al., 2025).

Despite its economic importance, ASM is widely associated with substantial environmental degradation and public health concerns. The most severe environmental impacts include deforestation, soil degradation, siltation of rivers, and contamination of surface waters, particularly through the release of mercury during gold extraction processes (Telmer & Stapper, 2007). These impacts are further intensified in regions where mining activities occur informally and outside legally designated areas.

One of the regions most affected by ASM-related environmental change is the Amazon Basin, where ASGM has expanded rapidly over recent decades. In the Peruvian Amazon, and particularly in the Department of Madre de Dios, ASGM has been a dominant driver of deforestation, with more than 120,000 hectares of primary tropical forest lost between 1984 and 2017 (Caballero Espejo et al., 2018). As Peru's largest gold-producing region, Madre de Dios has experienced rapid growth in ASM activities, many of which encroach upon forestry concessions, protected areas, and Indigenous territories (Becerra et al., 2024). The severity of environmental degradation and associated human rights concerns prompted the Peruvian government to launch Operation Mercury in 2019, a large-scale intervention aimed at curbing illegal mining in the La Pampa corridor (Becerra et al., 2024; Dethier, Silman, Fernandez, et al., 2023).

Monitoring ASM activities in remote and densely forested regions such as Madre de Dios presents significant logistical and technical challenges. Traditional field-based surveys are often constrained by the large spatial extent of mining areas, difficult terrain, limited accessibility, and ongoing security concerns, which restrict the availability of reliable ground truth data (Nava et al., 2022; Pasanisi et al., 2025). As a result, satellite-based RS has become an essential tool for observing, mapping, and monitoring ASM activities at regional to national scales.

ASM features observable in satellite imagery typically appear as clusters or ribbons of excavation pits, mining ponds, exposed sediments, and bare-earth waste piles located along river networks (Owusu-Nimo et al., 2018; Snapir et al., 2017). These features exhibit distinctive spectral characteristics, including high reflectance in near-infrared bands and strong contrast with vegetation in short-wave infrared wavelengths (Gallwey et al., 2020). However, ASM sites can also exhibit spectral and spatial similarities to other land-cover types, such as water bodies, sand-mining areas, or urban settlements with reflective rooftops, complicating accurate detection and delineation (Ofori-Ampofo et al., 2025).

To address these challenges, recent research has increasingly explored advanced image analysis techniques based on DL. Convolutional neural networks, particularly segmentation-based architectures such as U-Net, have demonstrated strong potential for capturing complex spatial patterns and contextual information in remotely sensed imagery (Jiang et al., 2024). ASM studies applying U-Net models with Sentinel-2 multispectral imagery have shown promising results for multitemporal ASM mapping and environmental change detection in various geographic contexts (Gallwey et al., 2020; Nava et al., 2022; Ofori-Ampofo et al., 2025). For instance, Ofori-Ampofo et al. (2025) applied DL and sentinel images for ASM classification and achieved an IoU of 75%, however, this research was confined to a single geographical area (Ghana) and do not consider how transferability of these models because, the broader applicability of these methods remains limited by challenges related to data availability and regional variability different environmental and mining contexts.

This suggests the need to investigate segmentation-based DL approaches for ASM detection and highlights the need to evaluate their effectiveness and transferability across different geographical areas as discussed by Ofori-Ampofo et al. (2025).

1.3 Literature Review

1.3.1 Artisanal Small-Scale Mining (ASM)

ASM is characterized by labor-intensive, low-tech mineral extraction and processing performed by individuals, families, or cooperatives, typically using rudimentary tools and non-mechanized methods (Gallwey et al., 2020; Ngom et al., 2023). Globally, ASM is most prevalent in regions of Latin America, Africa, and Asia, and is a major contributor to the global mineral supply, including approximately 20% of gold and diamonds, and up to 80% of sapphires (Couttenier et al., 2022). While gold mining has historically garnered the most research attention due to its simple extraction methods and easy market access, other commodities such as diamonds, cassiterite, and cobalt also play significant roles in the sector (Ngom et al., 2020; Nursamsi et al., 2024).

In South America, particularly in Madre de Dios, Peru, ASM has become one of the most prominent hotspots, especially for gold mining. The rapid growth of ASM in this region has been driven by factors such as global gold prices, poverty, and limited access to formal employment (Caballero Espejo et al., 2018). The completion of the Interoceanic Highway in 2012, which connects Madre de Dios to Brazil, further facilitated access to previously remote areas, accelerating the spread of ASM (Asner et al., 2010; Asner & Tupayachi, 2016). This expansion, while contributing to local economies, has led to significant environmental degradation, including alarming rates of deforestation, often linked directly to the growth of ASM activities (Asner et al., 2013; Caballero Espejo et al., 2018).

However, the informal and often illegal nature of ASM presents substantial challenges. In Madre de Dios, for instance, the lack of formal regulation, combined with high levels of illegal mining, has created an environment marked by poor governance, corruption, and weak law enforcement. This has hindered the implementation of effective policies by national governments and international organizations aimed at mitigating the negative impacts of mining (USAID, 2020). Despite these challenges, ASM remains a vital source of income for many, operating across a spectrum of formality, from illegal operations in protected areas to licensed, environmentally compliant ventures (Gallwey et al., 2020; Ofori-Ampofo et al., 2025).

1.3.2 Impact of Artisanal Small-Scale Mining (ASM)

1.3.2.1 Environmental Impacts

Artisanal Small-Scale Mining contributes significantly to environmental degradation, particularly in the Amazon and regions like Madre de Dios, Peru. One of the primary environmental impacts of ASM is deforestation. Over a period of 34 years (1984–2017), ASM led to the loss of more than 95,000 hectares of forest in Madre de Dios (Caballero Espejo et al., 2018). Between 2010 and 2017, deforestation from ASM more than doubled, with 64,586 hectares lost during this period alone, compared to 1985-2009 (Caballero Espejo et al., 2018). This destruction is compounded by infrastructure development, such as road building, which facilitates the expansion of mining activities and accelerates land cover change (Asner et al., 2013).

ASM also exacerbates soil erosion, particularly in regions like the Colorado River watershed, due to the disruption of soil during mining operations (Diringer et al., 2020). In addition, the widespread use of mercury in gold extraction has led to severe contamination of both soils and waterways. The influx of mercury from artisanal mining is considered the largest source of mercury pollution in Madre de Dios, affecting water, soil, and local biota (Gerson et al., 2022). This contamination results in the bioaccumulation of mercury in fish and wildlife, posing risks to human health, especially for local populations who rely on these resources for sustenance.

Biodiversity loss is another significant consequence of ASM. The deforestation and contamination of soils and water resources threaten the rich ecosystems of the Amazon Rainforest, particularly in Madre de Dios (Asner et al., 2013). In areas like the Los Amigos Conservation Concession, mercury deposition from ASM has intensified, raising concerns about the long-term survival of species and the overall ecological health of the region (Gerson et al., 2022).

1.3.2.2 Human Health Impacts

Mercury exposure is one of the most concerning health risks for ASM communities. Miners are frequently exposed to elemental mercury during the amalgamation process, leading to toxic vapor inhalation (Diringer et al., 2020). This exposure is linked to neurological and developmental disorders, particularly in pregnant women and children (Gerson et al., 2022). Additionally, communities living downstream of ASM areas face significant risks from dietary mercury exposure due to the contamination of local fish populations (Caballero Espejo et al., 2018).

In Madre de Dios, mercury contamination has resulted in a public health crisis, with increasing cases of mercury poisoning and respiratory illnesses (Diringer et al., 2020). Despite the Peruvian government's efforts to address mercury contamination through states of emergency, enforcement of policies remains a major challenge, leading to chronic health issues among miners and nearby populations (Diringer et al., 2015, 2020).

1.3.2.3 Social and Economic Impacts

The informal and unregulated nature of the sector creates economic instability and limits opportunities for sustainable growth. The sector's informality also means that much of the revenue generated from ASM remains unaccounted for, undermining economic development (Caballero Espejo et al., 2018).

Labor conditions in ASM are often harsh, with workers subjected to exploitation and violence. Women, who account for up to 50% of the workforce, are often given the most physically demanding and poorly paid tasks, such as panning and washing for gold (USAID, 2020). Gender-based violence (GBV) is also prevalent in mining camps, where women face significant risks due to a lack of rights awareness and inadequate protection (USAID, 2020). Furthermore, child labor remains widespread in ASM sites, exposing minors to hazardous conditions, including mercury poisoning (Gerson et al., 2022).

Governance challenges further complicate the regulation of ASM. Many ASM activities are illegal, operating outside the formal economy and often leading to conflicts over land tenure and resource rights (Asner et al., 2013). The weak enforcement of environmental laws, combined with corruption, has allowed the sector to remain largely informal, preventing the government from effectively managing or regulating mining activities (USAID, 2020). In regions like Madre de Dios, these issues are compounded by conflicts between ASM miners and large-scale industrial mining companies over land rights, exacerbating environmental degradation and fueling violence (Caballero Espejo et al., 2018).

1.3.3 Remote Sensing for Artisanal Small-Scale Mining (ASM) Detection

Monitoring ASM presents significant challenges due to the scarcity of reliable ground truth data for accurately identifying mining locations (Pasanisi et al., 2025). Armed conflicts and intercommunity tensions in many ASM regions further hinder field-based data collection, emphasizing the need for RS-based approaches to detect, monitor, and inventory ASM activities effectively (Nava et al., 2022). Satellite imagery has become a valuable tool for detecting and mapping ASM activities, especially in identifying mining ponds and residual water bodies formed through sediment extraction, a hallmark of small-scale gold mining (Caballero Espejo et al., 2018; Camalan et al., 2022).

These mining ponds shown in (Figure 1.1), typically referred to as lagoons, are shallow water bodies formed during sediment excavation for gold processing. The ponds exhibit distinct visual characteristics that vary depending on the level of mining activity: deep green tones indicate inactive areas, lighter green hues mark transitional sites, and chalky clay-colored waters signal active mining operations (Becerra et al., 2024; Camalan et al., 2022). ASM sites are predominantly surface-based and alluvial in nature, often manifesting as linear or clustered arrangements of excavation pits situated near river systems, frequently accompanied by dry pits and exposed waste piles (Snapir et al., 2017; Owusu-Nimo et al., 2018). These sites vary in size, from areas smaller than half a hectare to large clusters covering several hundred hectares (Gallwey et al., 2020).

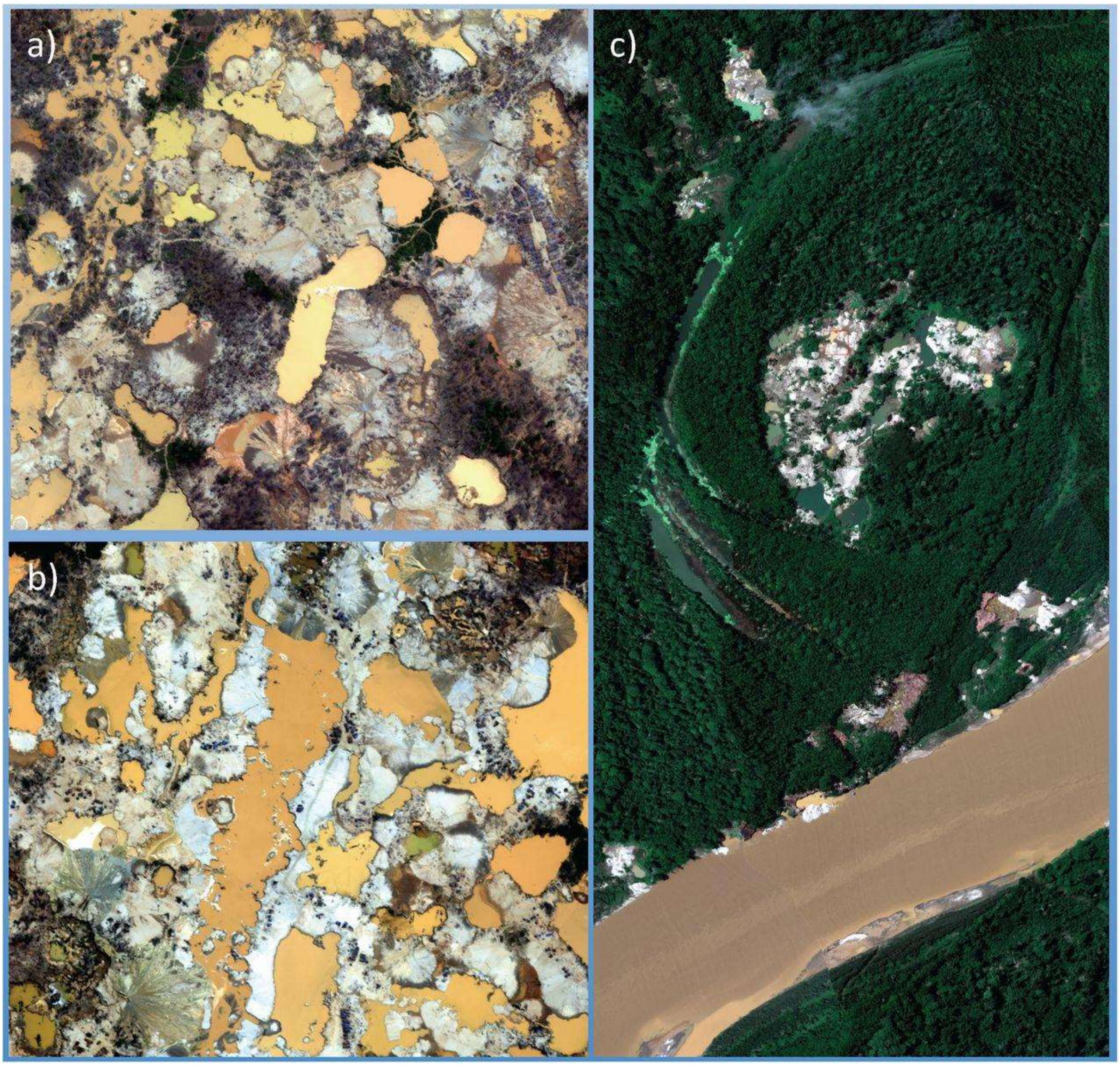

Figure 1.1 – (A–B) Images showing internal conditions within the Guacamayo and Huepetuhe mining sites. (C) Image showing ASM activities located both along and at a distance from the banks of the Madre de Dios River. Across all examples, the mining landscapes are characterized by widespread, heterogeneous patches of exposed soil mixed with stagnant water bodies(ponds) formed as a result of ASM practices (Asner et al., 2013).

Traditional RS approaches, which have utilized optical and radar data for ASM detection, encounter notable limitations, particularly the scarcity of publicly available ASM reference datasets (Ofori-Ampofo et al., 2025). Moreover, open-access datasets tend to focus on large-scale mining operations, whose spatial and spectral characteristics differ significantly from those of ASM sites, thus limiting the generalizability of the data (Ofori-Ampofo et al., 2025). Despite these challenges, RS offers a cost-effective alternative to traditional field surveys, enabling broad spatial coverage and regular, repeatable observations (Toth & Jóźków, 2016). Satellite platforms can acquire data consistently, supporting continuous monitoring of mining activities (Nugroho et al., 2024).

The use of high-resolution satellite sensors such as Sentinel-2 has proven particularly effective in detecting ASM activities. With a 10 m resolution and specialized spectral channels, such as the Vegetation Red Edge (VRE) and Near Infrared (NIR) bands, Sentinel-2 provides superior performance in discriminating ASM from other land covers (Gallwey et al., 2020; Nyamekye et al., 2021). Additionally, synthetic aperture radar (SAR) sensors like Sentinel-1 and TerraSAR-X are essential for monitoring ASM in cloud-prone regions, as they are weather-independent and can detect surface structural changes and texture through backscatter and InSAR coherence analysis. These sensors are particularly useful for identifying in-channel dredges or surface deformation resulting from underground mining (Alessi et al., 2023; Becerra et al., 2024; Nugroho et al., 2024).

Remote sensing indices, such as the Normalized Difference Vegetation Index (NDVI), Modified Normalized Difference Water Index (MNDWI), and Normalized Difference Built-up Index (NDBI), are frequently employed to enhance ASM detection. NDVI is widely used to detect vegetation loss, while MNDWI and NDBI are particularly useful for delineating mining ponds and associated settlements (Cui et al., 2022; Kimijima et al., 2021; Madasa et al., 2021; Nyamekye et al., 2021). Despite the potential of RS technologies, the informal nature of ASM and its often undocumented, remote locations complicate detection, particularly at coarse resolutions (Gallwey et al., 2020; Ngom et al., 2023). In tropical regions like Ghana or the Democratic Republic of Congo (DRC), persistent cloud cover further limits the effectiveness of traditional optical satellite sensors (Gallwey et al., 2020; Nyamekye et al., 2021; Pasanisi et al., 2025).

1.3.4 Deep Learning for Artisanal Small-Scale Mining Detection

The monitoring and delineation of deforestation associated with ASM is an essential application within broader land use and land cover (LULC) mapping. Traditional LULC mapping approaches often use pixel-based classification techniques that rely on the spectral characteristics of target classes, typically implemented via machine learning classifiers (Gallwey et al., 2020). However, convolutional neural networks (CNNs) have demonstrated superior performance over conventional methods such as Random Forests

(RF) and Support Vector Machines (SVM) (Nyamekye et al., 2021), particularly in ASM extent mapping.

Deep learning, especially CNN-based architectures, has substantially enhanced the ability to monitor LULC changes at finer spatial and thematic scales, enabling the segmentation and labeling of individual objects within remotely sensed imagery. CNNs have emerged as particularly effective for detailed spatial analysis, with the ability to capture hierarchical feature representations and spatial dependencies (Camalan et al., 2022c; Gallwey et al., 2020).

In the context of ASM, satellite imagery presents challenges, as artisanal gold mining sites may exhibit visual similarities to sand-mining areas or urban settlements, often due to highly reflective surfaces. Their spatial configurations are frequently circular and align with riverine networks, further complicating discrimination from other land-cover types (Ofori-Ampofo et al., 2025). This is particularly evident in true-color composite imagery, where ASM sites and surrounding land features can be difficult to distinguish due to their similar spectral signatures.

Recent advances in DL have significantly improved the accuracy and efficiency of ASM detection. CNN-based models like U-Net have been applied to remotely sensed data, enabling automated, high-resolution mapping of ASM activities and related environmental changes. For instance, Gallwey et al. (2020) and Nava et al. (2022) used U-Net in combination with Sentinel-2 multispectral imagery for multitemporal mapping of ASM activities in Ghana and Burkina Faso. Similarly, (Nugroho et al., 2024) employed U-Net with high-resolution synthetic aperture radar (SAR) data from TerraSAR-X to classify land cover types, including open-pit mining areas, vegetation, and water bodies, in Indonesia.

While pixel-based approaches remain common, they often lack spatial context and can result in "salt-and-pepper" noise or spectral confusion between bare soil in mines, urban areas, or cleared agricultural land (Gallwey et al., 2020; Simionato et al., 2021). In contrast, the Object-Based Image Analysis (GEOBIA) approach groups pixels based on spectral and geometric similarity, simulating human visual interpretation more effectively (Gallwey et al., 2020; Luethje et al., 2014). Research has shown that GEOBIA, combined with data mining techniques, can enhance ASM detection by analyzing textural and spatial attributes like entropy and area (Simionato et al., 2021).

Despite the success of traditional machine learning algorithms like RF and SVM in ASM detection (Camalan et al., 2022c; Gallwey et al., 2020), DL methods, particularly CNNs like U-Net, are now preferred for their ability to automatically learn spatial dependencies and hierarchical features (Couttenier et al., 2022; Pasanisi et al., 2025). Advanced models, including Transformers and Foundation Models, are now being incorporated to capture long-range contextual dependencies, significantly improving the accuracy of mapping complex mining footprints in diverse global climates (Hong et al., 2025; Ofori-Ampofo et al., 2025; Pasanisi et al., 2025).

The integration of DL with RS has revolutionized ASM monitoring by providing scalable, automated alternatives to traditional field surveys, which are often labor-intensive and limited by the remote, mobile, and informal nature of ASM activities (Gallwey et al., 2020). These activities, which often occur in conflict-prone regions, require advanced computational strategies to address their small spatial footprints and spectral similarities to other land-cover types (Nursamsi et al., 2024; Pasanisi et al., 2025).

1.3.5 Transfer Learning for Enhanced Model Performance

Transfer Learning (TL) is a machine learning technique that leverages knowledge gained from a primary task (source domain) to improve performance on a secondary, related task (target domain) (Pires De Lima & Marfurt, 2019). It addresses the challenge of domain shift and reduces reliance on labeled data by transferring knowledge from a source domain to a target domain. This process is particularly beneficial when there is abundant data in the source domain but limited labeled data in the target domain. TL aims to enhance the model's ability to generalize well to unseen data and perform tasks it has not encountered during training, thus improving both efficiency and accuracy.

Fine-tuned TL involves pre-training a model on the source domain (Ds) and subsequently fine-tuning it for a specific task in the target domain (Dt) (L. Ma et al., 2019). This method is effective in transferring learned features and knowledge from the source domain to the target domain, reducing the amount of data needed for training while enhancing model performance. The strategy’s effectiveness depends on several factors, including the availability of labeled data in both domains, the similarity between the source and target datasets, and the model's ability to adjust or share weights between tasks (Wurm et al., 2019). Fine-tuning these models with a smaller amount of labeled data from the target task leads to the development of more accurate and effective models (Li et al., 2020).

In this study, Madre de Dios, Peru, characterized by extensive ASM activity, was selected as the primary training area for the DL segmentation model and will be fine-tuned on a dataset from Kayapó (Brazil), also experiencing significant ASM-related land disturbance. These regional variations introduce domain shifts that can substantially affect the generalization ability of DL models. Therefore, this study investigates the extent to which a model trained in Madre de Dios can be directly transferred to Kayapó without retraining, and the performance improvements that can be achieved through TL by fine-tuning the pretrained model using a limited amount of labeled data from the target regions. This evaluation will provide insight into the spatial transferability of segmentation-based ASM detection models and their applicability for scalable monitoring across heterogeneous tropical environments.

1.3.6 RELATED WORK

Several studies have applied both traditional machine learning and DL approaches to classify ASM and associated land cover changes using multi- spectral satellite imagery. For instance, Nyamekye et al. (2021) applied a range of classifiers including artificial neural networks (ANN), SVM, RF, and CNNs on Sentinel- 2 data to map ASM landscapes in the Birim Basin, Ghana, demonstrating the efficacy of machine learning for high- accuracy ASM classification and highlighting the importance of spectral features such as the vegetation red edge (VRE) band in discriminating mining disturbances from natural vegetation. Kwang et al., (2025) also employed machine learning algorithms like RF, SVM, ANN, and Maximum Likelihood Classification (MLC) to assess the impact of ASM on forest vegetation. Their study found significant vegetation loss due to ASM and recommended using advanced machine learning techniques for more accurate land management and policy interventions.

Spectral and textural segmentation techniques have been shown to improve ASM detection accuracy. Fonseca et al. (2024) combined spectral and textural features from Landsat time series with RF classification and time-series segmentation (LandTrendr) to achieve high detection accuracy in the Brazilian Amazon, illustrating the benefit of incorporating texture alongside spectral information for discrimination of heterogeneous mining scars (Fonseca et al., 2024).

Complementary to classification efforts, DL has been leveraged for large‐ scale ASM mapping. Couttenier et al. (2022) implemented a CNN‐ based image segmentation framework in Sub‐ Tropical West Africa, showing that convolutional architectures can detect ASM signatures from Sentinel‐ 2 imagery, though highlighting challenges in recall when detecting smaller or spectrally ambiguous mining patches (Couttenier et al., 2022). Their work motivates the use of advanced segmentation networks in this study, as well as the exploration of TL strategies to adapt learned features to new geographic domains such as Kayapó. (Akpah et al., 2022) assessed the suitability of convolutional autoencoders (CAE) combined with UAV imagery for classifying legal versus illegal ASGM sites in Ghana. Their results showed that the CAE outperformed traditional classifiers, achieving an impressive 97.52% classification accuracy. This method is particularly useful for monitoring and controlling illegal mining activities in remote areas, where traditional monitoring approaches are ineffective.

Environmental impacts of mining and the need for robust detection methods have also been explored through long‐ term analyses of deforestation. Caballero Espejo et al. (2018) quantified ASM‐ linked deforestation in the Peruvian Amazon over several decades using Landsat time series, revealing substantial forest loss associated with mining expansion, and showcasing the importance of temporal RS analysis in understanding landscape transformation (Caballero Espejo et al., 2018).

In addition to optical imagery, multi‐ source data integration has been explored to characterize ASM dynamics. (Kimijima et al. (2021) employed a combination of Landsat optical data, nighttime light intensity, and precipitation records to assess mining camp evolution in Indonesia, demonstrating that auxiliary datasets can reveal socio‐ environmental drivers and proxies of mining expansion not captured by optical data alone (Kimijima et al., 2021).

Moreover, operational real‐ time monitoring approaches have been developed using synthetic aperture radar (SAR) to address cloud cover limitations common in tropical regions. Becerra et al. (2024) devised near real‐ time alerts for illegal gold mining using Sentinel‐ 1 SAR and a change detection algorithm , achieving high accuracies and proving the value of radar data in dynamic ASM surveillance (Becerra et al., 2024).

1.3.7 RESEARCH GAP

A key limitation lies in the limited availability of reliable and publicly accessible ground truth datasets for ASM detection. Many ASM activities occur in remote, insecure, or politically sensitive regions, where field-based data collection is restricted by difficult terrain, safety concerns, and limited institutional capacity (Nava et al., 2022; Pasanisi et al., 2025). Numerous studies result in manually digitizing labels from aerial images. This scarcity of reference data hampers the reproducibility of existing studies and restricts the development, validation, and operational deployment of robust ASM detection models (Ofori-Ampofo et al., 2025).

A gap in the current literature concerns the transferability and generalization of segmentation-based ASM detection models. Environmental conditions, land-cover composition, mining practices, and spectral characteristics vary substantially across regions such as Madre de Dios in Peru and the Kayapó region in Brazil. Models trained in one geographic context may therefore experience performance degradation when applied to unseen regions. However, the extent of this degradation and the factors influencing model transferability have not been sufficiently examined.

Furthermore, the potential of TL strategies to address these challenges remains underexplored in the context of ASM detection. While TL has shown promise in other RS applications (Wurm et al., 2019), studies have not investigated the effectiveness for ASM model generalization and transferability across regions. This gap limits the development of scalable and reusable monitoring frameworks capable of supporting near real-time ASM surveillance across multiple geographic contexts. This research seeks to address this gap by determining whether fine-tuning an ASM pretrained segmentation model of a given location can improve ASM detection performance in new regions compared to direct model transfer without adaptation.

Addressing these research gaps is essential for advancing robust, transferable, and operational ASM monitoring systems that can support environmental governance, policy enforcement, and sustainable land management across the Amazon Basin and beyond. This thesis aims to contribute to this emerging research area by systematically evaluating segmentation-based DL models for ASM detection in Madre de Dios and by assessing their transferability and performance improvement through transfer learning when applied to the Kayapó region in Brazil.

1.3.8 Research Questions and Objectives

To achieve the overall research aim, the study is guided by the following research questions

- How effectively can a segmentation-based deep learning model trained on Sentinel-2 imagery detect and delineate ASM in Madre de Dios, Peru?

- To what extent can the Madre de Dios model be transferred to Kayapó without retraining (direct model transfer)?

- How does transfer learning (fine-tuning) improve ASM segmentation detection performance in Kayapó compared to direct model transfer?

This research has three objectives and they are as follows.

- To evaluate the effectiveness of a segmentation-based DL model trained on Sentinel-2 imagery for detecting and delineating ASM activities in Madre de Dios, Peru.

- To assess the transferability of a segmentation-based ASM detection model trained in Madre de Dios when applied to the Kayapó region in Brazil without fine-tuning.

- To evaluate the impact of TL through fine-tuning on ASM detection performance in the Kayapó region.

1.3.9 Contributions and Significance of the Study

1.3.9.1 Scientific Contributions

The research addresses the underexplored issue of model transferability in ASM detection. While previous studies have demonstrated the potential of DL models for mapping ASM in individual regions, few have assessed how well these models generalize when applied to geographically and environmentally distinct areas. The study contributes to the emerging application of TL in RS–based ASM monitoring. By comparing direct model transfer with TL through fine-tuning, the research evaluates the extent to which pretrained segmentation models can be adapted to new regions using limited training data. This analysis offers insights into the effectiveness of TL strategies for improving model robustness and scalability, addressing a critical gap in current literature.

1.3.9.2 Practical and Societal Significance

Beyond its scientific contributions, this study holds significant practical relevance for environmental monitoring, policy implementation, and sustainable land management. Accurate and timely detection of ASM activities is essential for mitigating deforestation, reducing mercury pollution, and protecting biodiversity and human health in vulnerable regions such as the Amazon Basin. The proposed DL framework supports near real-time monitoring capabilities that can enhance the ability of governments, environmental agencies, and non-governmental organizations to identify and respond to illegal mining activities.

The focus on transferability and model reuse further increases the operational value of the proposed approach. Developing ASM detection models that can be adapted across regions reduces the need for extensive region-specific data collection, which is often constrained by logistical, financial, and security limitations. As a result, the findings of this study support the development of scalable and cost-effective monitoring systems capable of being deployed across multiple geographic contexts. This research also contributes to broader efforts to promote sustainable development, strengthen environmental governance, and support evidence-based decision-making in resource-dependent regions.

2. METHODOLOGY

Figure 2.1 is the methodological flowchart representing the sequence of steps used in this study. It outlines the key stages from data acquisition to model evaluation and transfer learning.

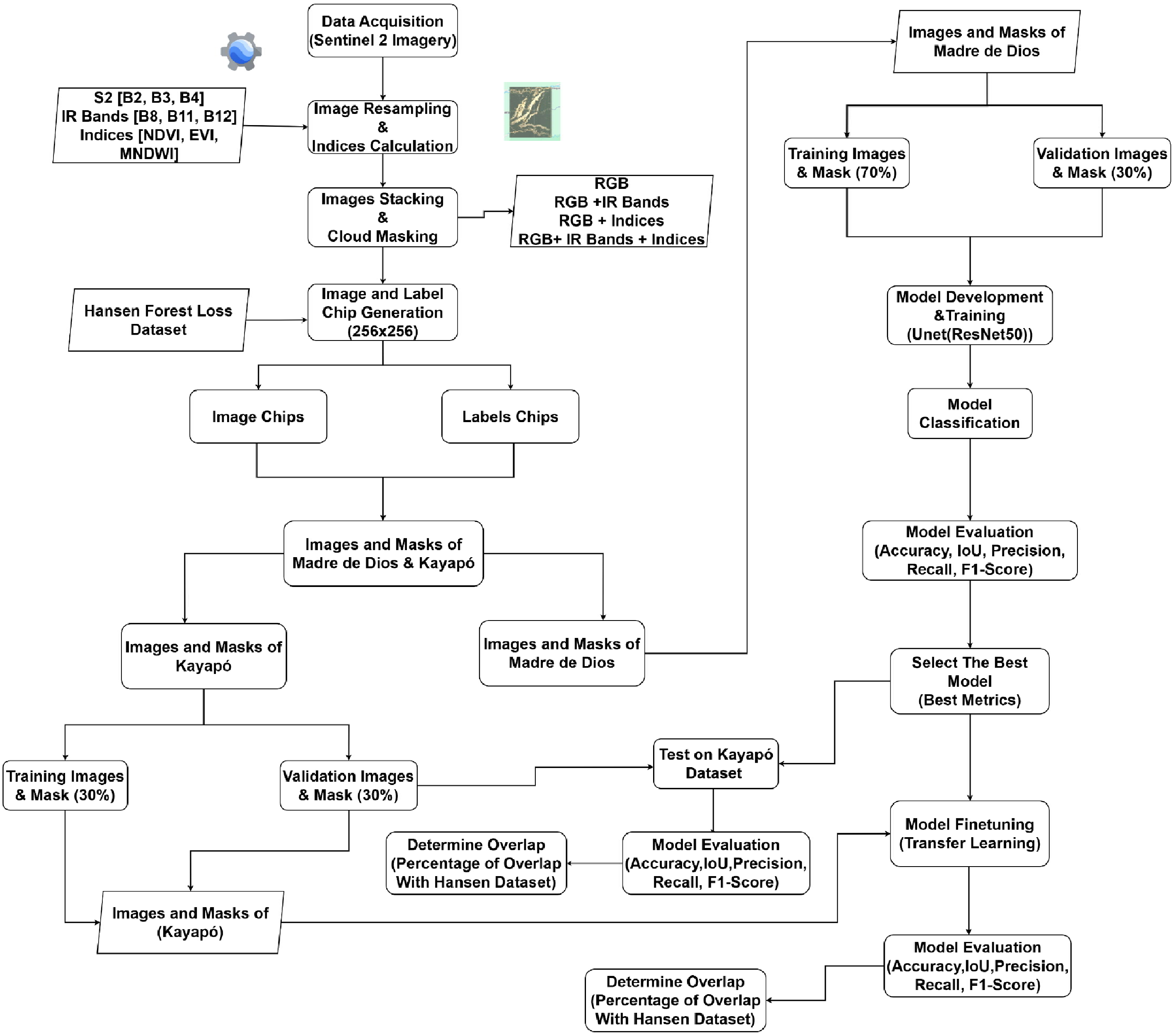

Figure 2.1 – Methodological flowchart of study.

2.1 STUDY AREA

2.1.1 MADRE DE DIOS, PERÚ.

Madre de Dios is a department located in the southeastern region of Peru, within the Amazon Basin, bordered by Brazil, Bolivia, and the Peruvian departments of Puno, Cusco, and Ucayali. As Peru's third-largest department, it spans a predominantly forested landscape, with its population concentrated in the city of Puerto Maldonado, situated at the confluence of the Madre de Dios and Tambopata rivers. The region is connected to Cusco via the Interoceanic Highway, a key transportation corridor that has facilitated increased access to previously remote areas (Ashe, 2012; Wikipedia, 2026).

Madre de Dios is renowned for its biodiversity, hosting the Manu National Park, the largest national park in Peru, covering approximately 1,700,000 hectares and designated as a World Heritage Site by UNESCO (Terra-i, 2013). Despite its ecological significance, the region has faced increasing pressures from intensive resource extraction, particularly from gold mining. Peru ranks as the largest gold exporter in South America and the fifth largest globally, underscoring the economic importance of gold mining alongside its environmental consequences (Markham & Sangermano, 2018).

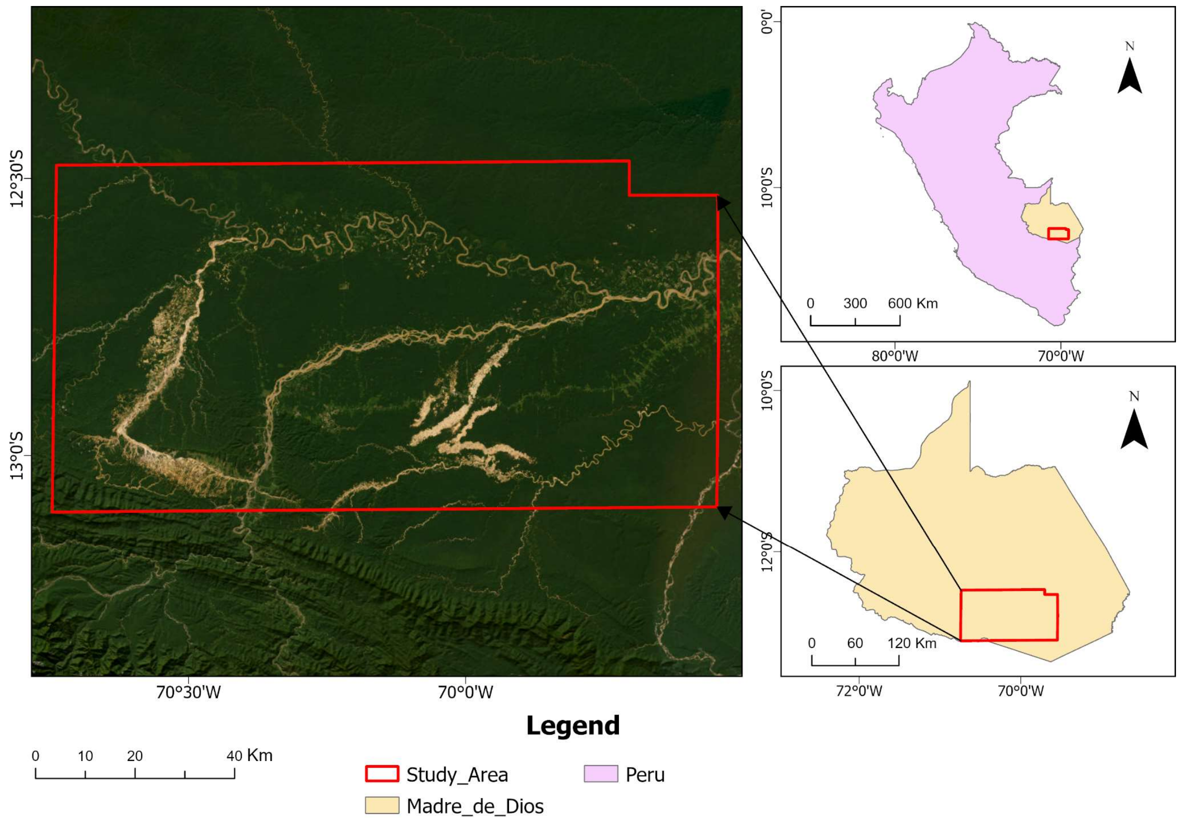

Figure 2.2 – Map of the study area in Madre de Dios.

Gold mining, particularly ASGM, has expanded dramatically since the 1980s, contributing to severe environmental degradation, including deforestation and contamination of local ecosystems (Swenson et al., 2011). The surge in gold prices following the 2008 global financial crisis further intensified this growth, with the region becoming the primary hotspot for illegal alluvial gold mining in Peru (Asner & Tupayachi, 2016; Swenson et al., 2011). This expansion was also facilitated by the completion of the Interoceanic Highway in 2011, which improved accessibility and opened previously remote areas to intensified gold exploitation (Nicolau et al., 2019; Saka et al., 2024).

Findings from Terra-i, (2013), supported by Swenson et al. (2011), showed that mining in Madre de Dios has contributed to deforestation at a faster rate than any other activity. Between 2003 and 2009, roughly 7,000 hectares of pristine forest and wetlands were cleared on two large mining sites, with deforestation accelerating in the last three years of the period. Despite the smaller size of wood extraction areas in Madre de Dios compared to regions like Ucayali and Loreto, the highest increases in habitat change were observed in this department (Terra-i, 2013).

Mercury, a toxic substance commonly used in ASGM operations to amalgamate and separate gold, has further exacerbated environmental and public health concerns. Incomplete mercury recovery during mining leads to substantial releases of mercury into the environment, contaminating soils and aquatic systems (Diringer et al., 2020). Since ASGM activities in Madre de Dios are often unregulated, the precise number of illegal miners remains unknown, but aerial imagery has shown significant and ongoing expansion of mining zones (Ashe, 2012; Swenson et al., 2011). Figure 2.2 shows a map of the study area affected by ASM within Madre de Dios.

As the largest gold-producing region in Peru, Madre de Dios presents substantial potential for mitigating mining-related deforestation at the national level. Timely monitoring, accurate mapping, and the effective dissemination of information to relevant stakeholders are critical to reducing the adverse impacts of mining on the Amazonian ecosystem, water quality, and human health (Becerra et al., 2024). Historically, the lack of near real-time monitoring for illegal mining has hindered both research and policy responses to address these issues.

The intensive mining activities in Madre de Dios, particularly within the ASGM sector, have led to significant political instability, human rights violations, and environmental damage. The Peruvian government has made efforts to address these concerns, with Madre de Dios becoming the focal point of national efforts to combat illegal mining. These efforts include dismantling illegal mining schemes, increasing law enforcement, and strengthening environmental protections (USAID, 2020).

2.1.2 KAYAPÓ, BRAZIL.

The Kayapó Indigenous Land (KIL), located along the Xingu River in the eastern part of the Amazon rainforest, covers approximately 11,350,000 hectares and is considered one of the largest tropical protected areas globally (Wikipedia, 2026a). It is home to the Kayapó people, whose scattered villages, ranging from 100 to 1,000 individuals, reside in tropical rainforest and savannah ecosystems. The Kayapó tribe has historically faced significant threats to their land and resources, primarily from illegal gold mining, logging, and agribusiness (Ej Atlas, 2023).

The Brazilian Federal Government officially established the KIL in 1991, covering roughly 3.3 million hectares of native forest in southern Pará. Despite its vast size, the KIL is situated within the "Arc of Deforestation," an area heavily affected by illegal mining operations (Ej Atlas, 2023). Mining activities, often illegal, have caused substantial environmental damage, including deforestation, water pollution from mercury and other heavy metals, soil degradation, and the destruction of local fauna. These activities have intensified over the years, driven by rising gold market prices (Ej Atlas, 2023).

Coordinated efforts by Indigenous groups, advocacy organizations, and the Brazilian government nearly eradicated mining activities in the Kayapó Preserve by 1994, following a mining and logging boom in the 1980s and early 1990s. This intervention resulted in nearly two decades without mining-related deforestation, and although revegetation was slow, suspended sediment concentrations (SSCs) in rivers returned to levels consistent with unaffected rivers in the region within less than a decade (Dethier, Silman, Fernandez, et al., 2023). However, since 2010, particularly from 2016 to the present, illegal mining activities have resurfaced in Kayapó territories, leading to significant deforestation and a resurgence in river SSCs, reminiscent of the levels observed during the mining boom of the 1980s and 1990s (Dethier, Silman, Leiva, et al., 2023).

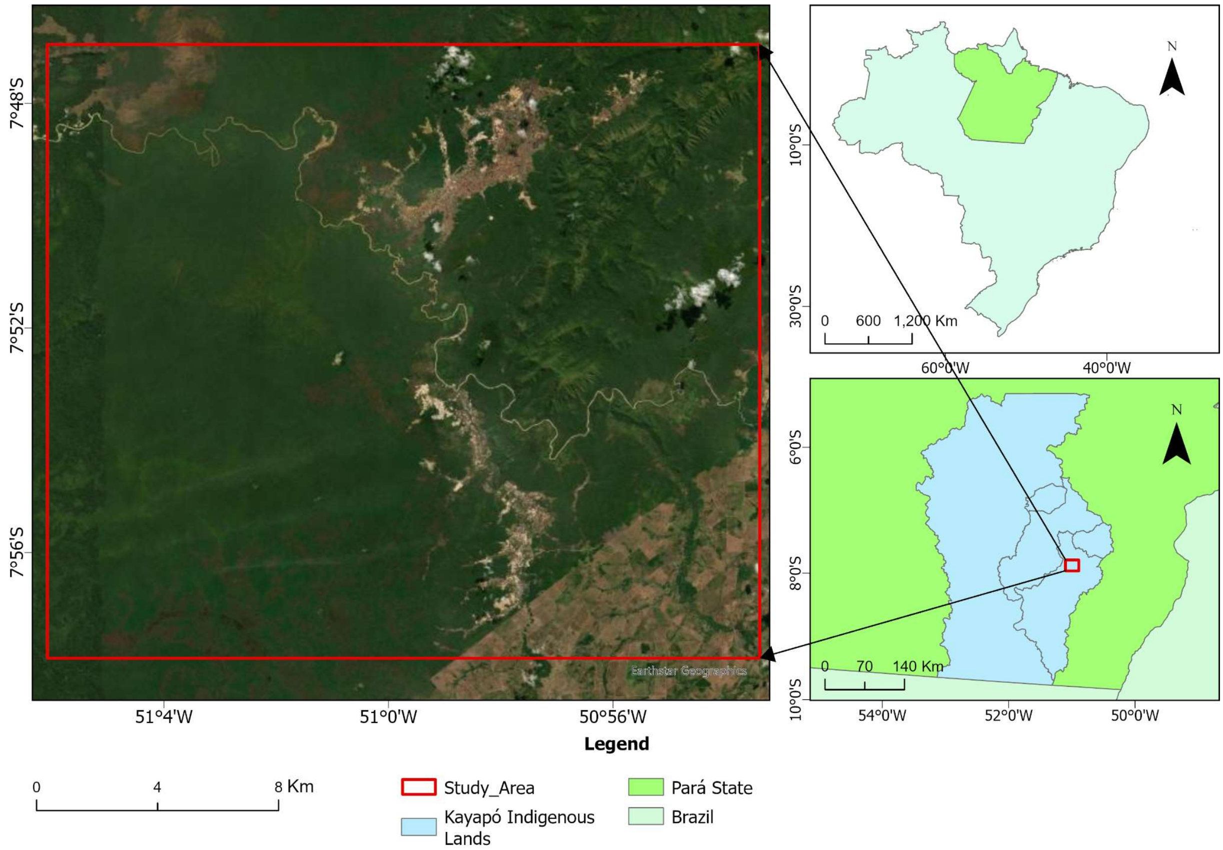

Figure 2.3 – Map of the study area in the Kayapó Indigenous Lands.

From 2012 to 2022, the area mined in Kayapó territory increased by 622%, from 19.1 km² to 137.8 km², reflecting the rapid expansion of illegal mining (Castro et al., 2025). Over the past two decades, illegal artisanal mining within Indigenous territories in the Brazilian Amazon has intensified, with an approximate 495% increase in the area occupied by mining from 2010 to 2020, particularly within Kayapó and Munduruku territories (Rjc et al., 2023). As a result, illegal mining has become one of the main drivers of deforestation in the region (Rorato et al., 2020).

The increasing threats from illegal mining within these Indigenous lands have prompted the Kayapó people to take action. Despite limited governmental protection, they have organized patrols of their territories, risking their lives to destroy bridges and remove mining machinery (Mataveli et al., 2022). Gold mining and logging near Kayapó communities have led to significant water pollution, introduced diseases like malaria, and disturbed the forest environment. Figure 2.3 shows a map of the study area affected by ASM considered within the Kayapó Indigenous Lands.

From a remote sensing perspective, ASM in Madre de Dios is predominantly characterized by mining features that form relatively large, contiguous, and spectrally distinct patches within dense, humid tropical forest (Asner & Tupayachi, 2016). The strong contrast between exposed soil, man made ponds, and intact vegetation enhances detectability in optical imagery (Elmes et al., 2014; USAID, 2020). The terrain is generally lowland and flat, with broad floodplains that facilitate the formation of extensive water-filled mining pits and sediment plumes, producing clear vegetation loss and moisture signals (Asner & Tupayachi, 2016; USAID, 2020).

In contrast, ASM in Kayapó tends to be more spatially fragmented and dispersed, often occurring along smaller tributaries within a more heterogeneous landscape that includes dense forest, secondary vegetation, and agricultural expansion zones. Disturbed areas may be partially obscured by rapid vegetation regrowth, reducing spectral separability. The presence of mixed disturbance signals from logging and pasture conversion further increases spectral confusion (da Silva et al., 2023; Ej Atlas, 2023). These structural and spectral differences between the two regions may introduce domain shift, directly affecting the generalization capacity of deep learning models trained in one region and transferred to another.

2.2 Data

2.2.1 Sentinel-2 Satellite Imagery

This study uses optical satellite imagery from the Sentinel-2 mission of the European Space Agency (ESA) as the primary data source for detecting ASM. Sentinel-2 consists of a constellation of two satellites (Sentinel-2A and Sentinel-2B) providing high-resolution, multi-spectral imagery with global coverage and a revisit time of five days at the equator (Drusch et al., 2012).

Sentinel-2 acquires data in 13 spectral bands spanning the visible, near-infrared (NIR), and shortwave infrared (SWIR) regions of the electromagnetic spectrum, with spatial resolutions of 10 m, 20 m, and 60 m. The availability of red, NIR, and SWIR bands makes Sentinel-2 particularly suitable for monitoring vegetation dynamics, soil exposure, and water characteristics, which are key indicators of ASM activity in tropical forest environments (Sonter et al., 2017; Zhu et al., 2017). Table 2.1 presents the spectral characteristics of Sentinel-2 bands used in this study.

Table 2.1: Sentinel-2 Spectral Bands and Characteristics

Sentinel-2 Bands	**Central Wavelength (nm)**	**Resolution (m)**
Band 1 – Coastal aerosol	443	60
Band 2 – Blue	490	10
Band 3 – Green	560	10
Band 4 – Red	665	10
Band 5 – Vegetation Red Edge	705	20
Band 6 – Vegetation Red Edge	740	20
Band 7 – Vegetation Red Edge	783	20
Band 8 – NIR	842	10
Band 8A – Vegetation Red Edge	865	20

Band 9 – Water vapour	945	60
Band 10 – SWIR – Cirrus	1375	60
Band 11 – SWIR	1610	20
Band 12 – SWIR	2190	20

Level-2A surface reflectance products were used in this study to ensure radiometric consistency and reduce atmospheric effects. These products are atmospherically corrected using the Sen2Cor processor and are widely used in land-cover and environmental disturbance mapping. The high spatial resolution of Sentinel-2 at 10 m enables the detection of medium-scale ASM features, such as mining pits, tailings, and sediment-laden water bodies, which are common in riverine mining contexts like Madre de Dios and the Kayapó region (Swenson et al., 2011).

Sentinel-2 imagery has been extensively used in previous studies for detecting deforestation, mining activities, and land-use change in the Amazon Basin, demonstrating its suitability for ASM monitoring at regional scales (Asner et al., 2013; Sonter et al., 2017). In this study, the 10 m resolution bands (B2, B3, B4, and B8) were primarily used for model training due to their finer spatial detail. Additionally, SWIR bands (B11 and B12) were incorporated for their sensitivity to soil exposure and moisture variations, which are critical for identifying mining pits and tailings. Derived spectral indices (NDVI, EVI, and MNDWI) were computed using combinations of these bands to enhance the discrimination of ASM features.

2.2.2 Hansen Global Forest Change Dataset

To support reference data preparation and contextual interpretation of mining-related disturbances, this study also utilized the Hansen Global Forest Change (GFC) dataset, a widely used global dataset that provides annual information on forest cover, forest loss, and forest gain at 30 m spatial resolution (Hansen et al., 2013).

The Hansen dataset is derived primarily from Landsat imagery and provides consistent, long-term records of forest change from the year 2000 onward. Forest loss in the dataset is defined as a stand-replacement disturbance, meaning the complete removal of tree canopy cover at a given pixel location (Hansen et al., 2013). This definition aligns well with the impacts of ASM, which often involves large-scale vegetation clearing and persistent land disturbance.

In this study, the Hansen forest loss layer was used to support the identification and validation of ASM-related deforestation patterns, particularly in regions where mining activities overlap with forest clearing. Previous research has demonstrated a strong spatial relationship between ASM expansion and forest loss in the Amazon, especially in riverine environments (Sonter et al., 2017; Swenson et al., 2011).

Although the Hansen dataset does not directly classify mining activities, it provides valuable contextual information that helps distinguish persistent mining-related disturbances from temporary or natural vegetation changes. The combination of Sentinel-2 imagery and the Hansen forest loss dataset therefore enable a more robust characterization of ASM impacts on forest ecosystems.

The combination of Sentinel-2 imagery and the Hansen Global Forest Change dataset offer complementary strengths for ASM detection and analysis. Sentinel-2 provides high-resolution, multi-spectral information suitable for learning spatial and spectral patterns of active mining areas, while the Hansen dataset offers a long-term perspective on forest disturbance associated with mining expansion.

Both datasets are freely available, globally consistent, and extensively validated in scientific literature, making them well suited for scalable environmental monitoring applications. Their combined use aligns with established practices in RS studies of mining and deforestation in tropical regions (Asner et al., 2013; Zhu et al., 2017).

2.3 DATA PROCESSING

The Sentinel-2 imagery was downloaded from Google Earth Engine (GEE), focusing on the Madre de Dios region for training and Kayapo for TL. The imagery used covers the period from January 2024 to July 2024, because those were the periods that had images with cloud cover less than 10%. To ensure the Sentinel-2 imagery is cloud free, the maskS2Clouds function in GEE is used to mask out pixels affected by clouds, using the Sentinel-2 Scene Classification Layer (SCL) band, which indicates cloud presence.

Sentinel-2 imagery is acquired at different resolutions (10m for RGB and NIR bands, 20m for SWIR bands), resampling was done to align all bands to the same spatial resolution. For this study, all bands are resampled to a uniform 10-meter resolution using the resample function in GEE, ensuring that all bands have the same spatial resolution.

To enhance the model's ability to detect ASM, vegetation indices are calculated from the Sentinel-2 imagery. Commonly used indices such as NDVI, EVI and MNDWI are essential in highlighting vegetation, deforestation and water bodies. MNDWI is included to improve the model’s ability to classify areas of clustered ponds because ASM leaves a traces of irregular shaped ponds in the mining areas

Given the lack of ground truth data, the Hansen Global Forest Loss dataset is utilized as label for regions where ASM activities are. This dataset is used to identify regions of deforestation, which are then linked to potential ASM activities since deforestation is commonly linked to illegal mining activities in many regions, including the Amazon. The forest loss datasets, available from Global Forest Watch, provides a global record of forest loss over time, including loss of tree cover for the years 2000–2024. The areas of forest loss within the Amazon Mining Watch (AMW) mining locations are clipped with three areas of study to be used as labels for the model training ensuring that only deforestation related to ASM are considered. AMW is a collaboration between Rainforest Investigations Network and Earthrise Media to map mining areas in the Amazon (Becerra et al., 2024).A binary mask is generated where 1 represents ASM (deforested) areas and 0 represents non-ASM areas (non-deforested) and thus they serve as training labels. Equation (1), Equation (2), and Equation (3) show the mathematical expression of NDVI, EVI, and MNDWI.

$$NDVI = \frac{(NIR - Red)}{(NIR + Red)} \quad (1)$$

- NIR = Near-Infrared Band (Band 8 for Sentinel-2)
- Red = Red Band (Band 4 for Sentinel-2)

$$EVI = G \times \frac{(NIR - Red)}{(NIR + C1 \times Red - C2 \times Blue + L)} \quad (2)$$

- NIR = Near-Infrared Band (Band 8 for Sentinel-2)
- Red = Red Band (Band 4 for Sentinel-2)
- Blue = Blue Band (Band 2 for Sentinel-2)
- G = Gain factor (default = 2.5)
- C1, C2 = Coefficients for the red and blue bands (default = 6 and 7.5, respectively)
- L = Canopy background adjustment (default = 100)

$$MNDWI = \frac{(Green - SWIR)}{(Green + SWIR)} \quad (3)$$

- Green = Green Band (Band 3 for Sentinel-2)
- SWIR1 = Short-Wave Infrared Band (Band 11 for Sentinel-2)

To train the model, the raw satellite imagery was broken into smaller image chips of 256x256 size. Each chip is typically associated with a corresponding label chip, which contains the ground-truth information(ASM areas). These image chips and label chips are used as input-output pairs for model training. For the source region, Madre de Dios (Peru), a total of 1,684 image–mask pairs were generated. These were randomly partitioned using a 70:30 split, resulting in 1,178 patches allocated for training and 506 patches for validation. For the target region, Kayapó (Brazil), 115 image–mask pairs were prepared following the same preprocessing procedure. These were similarly divided into 70% training (80 patches) and 30% validation (35 patches).

The Export Training Data for Deep Learning tool in ArcGIS Pro was used to generate the image and label chips. This tool was essential in preparing input data for the modeling, as it handles the extraction of chips from larger raster datasets and ensures that both images and labels are paired correctly.

The tool required the input satellite imagery, which in this case is the Sentinel-2 imagery (RGB, NIR, SWIR, etc.) and the label data, which is the ground truth (ASM area). In this study, labels are generated from the Hansen Global Forest Loss datasets, where areas of deforestation (potential ASM activities) are marked as 1, and other areas are marked as 0. The X and Y dimensions of the images were made to be 256x256 and zero was to as stride to avoid overlapping of images. This process was done for all images from the 3 study areas.

The Export Training Data for Deep Learning tool outputs the image chips and label chips in the 'TIF' format that is compatible with DL frameworks.

2.4 U-NET ARCHITECTURE

The U-Net model as shown in Figure 2.4 is characterized by a two-part architecture consisting of an encoder (left branch) and a decoder (right branch). At each resolution level, feature maps from the encoder are concatenated with corresponding feature maps in the decoder, facilitating the integration of spatial and contextual information (Giang et al., 2020). The encoder, or contracting path, follows a conventional convolutional network structure, involving repeated applications of two 3×3 convolutional layers, each followed by a Rectified Linear Unit (ReLU) activation function and a 2×2 max-pooling operation. The decoder, or expansive path, consists of a sequence of 2×2 up-convolutional layers, concatenation with the corresponding encoder feature maps, and two 3×3 convolutional layers with ReLU activation, concluding with a 1 × 1 convolution layer (Perez-Guerra et al., 2024; Ronneberger et al., 2015).

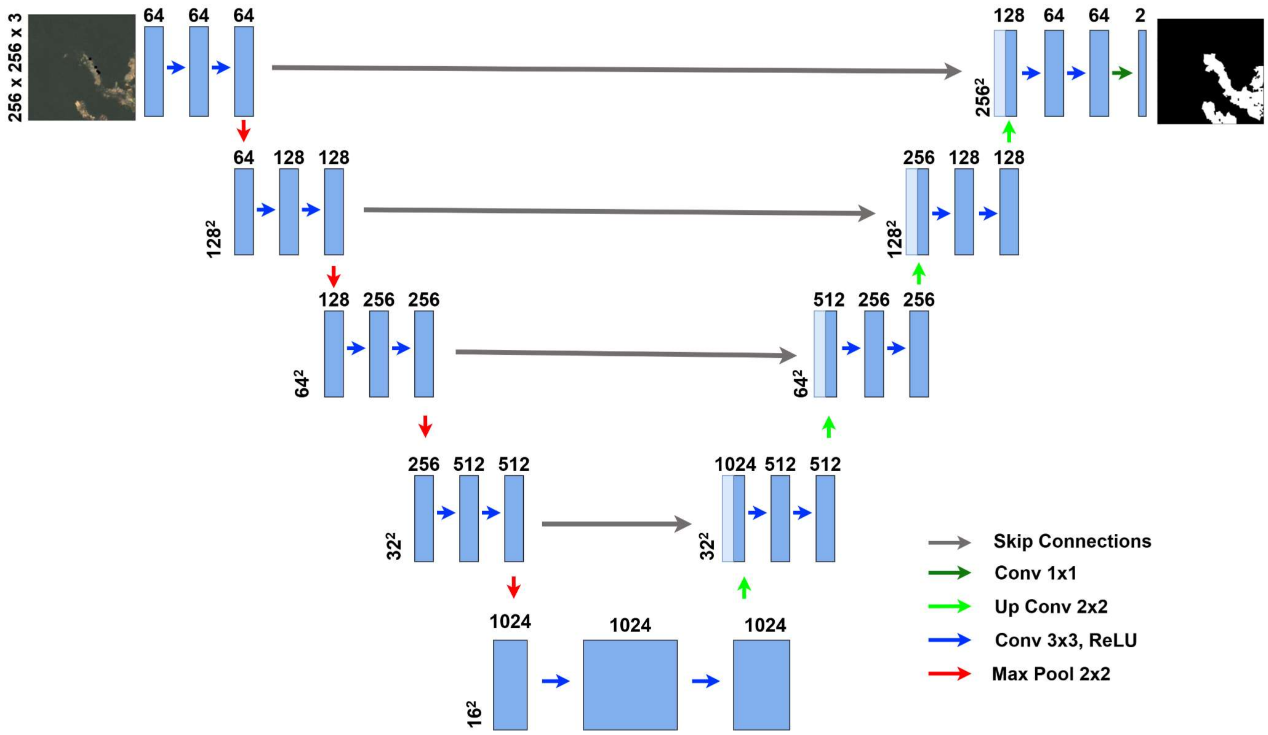

Figure 2.4 – Unet Architecture.

Most DL architectures, including U-Net, are composed of contraction and expansion paths, which are commonly referred to as the encoder and decoder. The encoder's role is to extract salient features while progressively reducing the spatial dimensions of the input image. In contrast, the decoder reconstructs the spatial resolution to enable accurate pixel-wise classification corresponding to the original input dimensions (de Moura et al., 2022).

This architecture has been widely adopted for semantic segmentation tasks, where individual pixels are associated with specific class labels, such as ASM and background in this study (Nava et al., 2022). Although Unet was introduced for medical image segmentation, it was selected for this study because it has consistently demonstrated a strong performance in remote sensing segmentation tasks involving mining and slums detection (Hejmanowska et al., 2025; Nugroho et al., 2024; Saputra et al., 2025; Wurm et al., 2019).

2.4.1 SMP Library using ResNet-50 Encoder

This study employs the Segmentation Models PyTorch (SMP) library, which offers a flexible and user-friendly framework for state-of-the-art segmentation architectures with configurable pretrained encoders (Iakubovskii, 2019). The SMP library includes a diverse collection of pretrained encoders, commonly known as backbones, for segmentation models. Instead of relying solely on features extracted from the final classification layer, the library utilizes intermediate feature representations passed to the decoder, ensuring more accurate segmentation (Iakubovskii, 2019).

For this study, the SMP implementation of U-Net was trained using a ResNet-50 encoder without pretrained weights, with the encoder depth fixed at five. The ResNet-50 encoder was selected for its proven performance in extracting meaningful features, which can then be passed to the decoder for precise segmentation.

Recent studies have shown the effectiveness of U-Net with ResNet-50 for semantic segmentation. For example, Perez-Guerra et al. (2024) demonstrated that the U-Net architecture, using ResNet-50 and ResNeXt-50 (32×4) encoders, achieved optimal performance for land cover segmentation using Sentinel-2 imagery, reporting an accuracy of 89% and a mean Intersection over Union (mIoU) of 74%. Similarly, research focused on river segmentation tasks highlighted the success of U-Net models combined with pretrained backbones, such as ResNet-50, which consistently outperformed other architectures in segmentation and width estimation tasks. The use of multiscale encoders and dense skip connections within U-Net ensured the preservation of fine-grained edge details while maintaining high-level contextual information (Daroya et al., 2025).

2.4.2 EXPERIMENTAL SETUP

The experimental setup for this study was designed to evaluate the performance of a segmentation-based DL model trained to detect ASM using Sentinel-2 imagery. The methodology involved training the model on a source region (Madre de Dios, Peru), followed by TL experiments applied to a target region (Kayapó, Brazil). The model was trained using a combination of 6 spectral bands (red, green, blue, NIR, SWIR1 and SWIR2), as well as indices (NDVI, EVI and MNDWI). The experiments were conducted on a cloud computing system equipped (Google Colab) with T4 GPU. These resources provided the necessary computational power for handling the large volumes of satellite imagery and DL model training. The model was implemented in Python using the SMP Library.

The performance of the model was evaluated using a combination of pixel-based accuracy metrics and spatial overlap analysis. The following metrics were used to assess the quality of the model's predictions: IoU, Accuracy, Precision, Recall, F1-Score.

2.3.3 MODEL TRAINING AND HYPERPARAMETER SELECTION

After several hyperparameter fine-tuning, the training procedure involved a batch size of 16, a learning rate of 1×10^{-4}, and early stopping to prevent overfitting. The number of epochs was set to 50, with performance monitored on the validation set to ensure convergence. The Adam optimizer was used to minimize the Binary Cross-Entropy with Logits (BCEWithLogitsLoss) loss function, which is suitable for binary classification tasks. The model's hyperparameters were fine-tuned based on validation performance.

2.5 BINARY CROSS-ENTROPY WITH LOGITS (BCEWITHLOGITSLOSS)

BCEWithLogitsLoss is a loss function that combines a Sigmoid layer with binary cross-entropy loss into a single function, enhancing numerical stability during training (Dong et al., 2025). This function is widely used in binary classification tasks, including binary semantic segmentation, as it directly handles the model's outputs in the form of logits, applying the Sigmoid function and then calculating the predicted probabilities along with binary cross-entropy loss (Xue & Zheng, 2024). By integrating both operations, BCEWithLogitsLoss reduces the risk of numerical underflow and improves gradient stability during training, making it particularly suitable for segmentation tasks. The BCEWithLogitsLoss function is mathematically defined in Equation (4).

$$L_{BCEWithLogits} = -\frac{1}{N}\sum_{i=1}^{N} [y_i \; log(\sigma(\hat{y}_i)) + (1 - y_i)log(1 - \sigma(\hat{y}_i))] \tag{4}$$

Where:

- y_i is the true binary label (1 for ASM, 0 for non-ASM),
- $\hat{y}_i$ is the predicted raw logits (before applying the sigmoid),
- $\sigma(\hat{y}_i)$ is the sigmoid activation function, which outputs a probability between 0 and 1 for each pixel,
- □is the number of pixels.

In this study, BCEWithLogitsLoss was employed to train the segmentation model. The dataset exhibited a significant class imbalance, with the background class occupying a much larger spatial extent compared to the target ASM class. This imbalance often leads to the model favoring the majority class, achieving high overall accuracy while underperforming in detecting the minority class (ASM). To address this issue, a positive class weighting strategy was introduced. The weight for the positive class was derived from the training masks to reflect the true distribution of the dataset, with the ASM class receiving a higher penalty for misclassification in proportion to its underrepresentation. This adjustment encouraged the model to learn more discriminative features for the minority class, improving recall and F1-score for ASM without the need for resampling or synthetic data generation.

2.6 OPTIMIZER: ADAM

The Adam optimizer is a widely used stochastic gradient descent-based optimization method that combines the benefits of both the adaptive gradient algorithm and root-mean-square propagation. It computes individual adaptive learning rates for each parameter by estimating the first and second moments of the gradients (Dastour & Hassan, 2023; Dong et al., 2025; Kingma & Ba, 2017). This makes the Adam optimizer particularly advantageous for applications with noisy data and sparse gradients, as it adapts the learning rate based on the data's characteristics (Kingma & Ba, 2017; Nava et al., 2022).

In this study, Adam was initialized with a learning rate of 1×10^{-4}, providing a stable balance between convergence speed and training stability. The optimizer was applied to all trainable parameters of the segmentation network, enabling efficient updates during backpropagation while reducing the likelihood of oscillations or divergence during early training stages. Following a study by (Kupcikevicius et al., 2025) , a learning rate scheduling strategy was implemented using the ReduceLROnPlateau scheduler to further enhance convergence. This scheduler monitors the validation loss during training and automatically reduces the learning rate when performance stagnates. Specifically, when the validation loss did not improve for five consecutive epochs (patience = 5), the learning rate was reduced by a factor of 0.5.

2.7 EVALUATION METRIC

In this study, model performance is evaluated using a set of standard classification and segmentation metrics: accuracy, precision, recall, F1- score, and Intersection over Union (IoU), all derived from the confusion matrix of predicted versus reference labels and widely used in semantic segmentation of remote sensing imagery. In the context of ASM detection, these metrics provide complementary perspectives on how well the segmentation model identifies and delineates mining areas within predominantly non- mined landscapes. Equation (5), Equation (6), Equation (7), Equation (8) and Equation (9) show the mathematical expression of Accuracy, Precision, Recall, F1-score and Intersection over Union (IoU).

Accuracy

Overall accuracy quantifies the proportion of correctly classified pixels over all pixels in the Sentinel- 2 scenes, that is, the sum of true positives and true negatives divided by the total number of pixels. Although accuracy is intuitive and frequently reported in RS studies, it can be misleading in highly imbalanced settings, where ASM occupies a small fraction of the area compared with intact forest and other land covers, because a model that predicts almost exclusively the majority (non- ASM) class can still yield a high overall accuracy.

$$Accuracy = \frac{TP+TN}{TP+TN+FP+FN} \quad (5)$$

where:

- TP (True Positive): Pixels correctly classified as ASM (mining area)
- TN (True Negative): Pixels correctly classified as non-ASM (non-mining area)
- FP (False Positive): Pixels incorrectly classified as ASM
- FN (False Negative): Pixels incorrectly classified as non-ASM

Precision

Precision for the ASM class measures the reliability of positive detections, defined as the proportion of predicted ASM pixels that are truly ASM (Fonseca et al., 2024; Li et al., 2020). High precision indicates that the model produces few false positives, meaning that non- mined features rarely misclassified as mining, which is important for avoiding unnecessary follow- up inspections and maintaining decision- makers' trust in the model outputs in Madre de Dios (Li et al., 2020).

$$Precision = \frac{TP}{TP + FP} \quad (6)$$

Recall

Recall (or sensitivity) for the ASM class quantifies the model's ability to detect actual mining pixels, defined as the proportion of true ASM pixels that are correctly classified as ASM. High recall implies that the segmentation model successfully identifies most mining areas, including small pits and narrow riverbank operations that are typical of artisanal gold extraction in Madre de Dios, which is critical because missed ASM detections (false negatives) directly translate into underestimation of mining extent and unmonitored environmental impacts.

$$Recall = \frac{TP}{TP + FN} \quad (7)$$

F1‐ score

The F1‐ score is the harmonic mean of precision and recall and provides a single indicator that balances omission and commission errors, making it especially useful in imbalanced classification problems such as ASM detection. In this thesis, the F1‐ score for the ASM class is used to compare different model configurations, for example, a baseline U‐ Net versus a U‐ Net with a ResNet‐ 50 encoder and different Sentinel‐ 2 band combinations and to select decision thresholds that balance correctly detecting mining areas with limiting false alarms (Wang et al., 2025).

$$F1 - score = 2 \times \frac{Precision \times Recall}{Precision + Recall} \quad (8)$$

Intersection over Union (IoU)

Intersection over Union (IoU), also known as the Jaccard Index, is a region‐ based metric that compares the overlap between predicted and reference segments for each class by dividing the area of intersection by the area of union (Li et al., 2020; Wang et al., 2025). It quantifies the degree of similarity between the predicted segmentation mask and the ground truth mask. IoU (and its average across classes, mean IoU) is widely used in DL‐ based semantic segmentation of RS images because it directly reflects the spatial agreement between predicted objects and ground truth, making it particularly suitable for evaluating the delineation of ASM areas (Fonseca et al., 2024; Li et al., 2020). In this work, the ASM‑ class IoU is a key metric for judging how accurately the U‑ Net with ResNet‑ 50 encoder delineates mining footprints in Sentinel‑ 2 imagery.

$$IoU = \frac{TP}{TP+FP+FN} \tag{9}$$

2.8 Zero-Shot Transfer Experiment

The zero-shot transfer experiment involved directly applying the pretrained model from Madre de Dios to the Kayapó region without any retraining. This approach was used to assess the generalization capabilities of the model and determine how well the learned features from the source domain could be applied to a new geographic area. The results were evaluated based on performance metrics (IoU, F1-score) and visual inspection of the segmentation output.

2.9 Transfer Learning (Fine-Tuning) Strategy

To enhance model generalization and adapt the segmentation model to the Kayapo dataset, a TL (fine-tuning) strategy was implemented. The U-Net architecture with a ResNet-50 encoder was used for fine-tuning, initialized with weights obtained from a model trained on the source dataset (Madre de Dios). These pretrained weights provided a robust initialization, enabling the network to leverage previously learned low-level and mid-level feature representations, while adapting to the spectral and spatial characteristics of the new dataset. This strategy allows the model to adapt to new spatial features (such as river morphology or forest structure) while retaining generalizable features learned in the source domain

Dataset Preparation and Augmentation

The Kayapo dataset consisted of six-band multispectral imagery and corresponding binary segmentation masks. The data were divided into training (70%) and validation (30%) subsets. To improve robustness and reduce overfitting, data augmentation was applied to the training set using geometric transformations and noise injection, such as horizontal and vertical flips, random 90° rotations, small shifts and scaling, limited rotations, and Gaussian noise (Thanapol et al., 2020). These augmentation strategies were chosen to preserve spectral integrity, avoiding color-based perturbations that would be unsuitable for multispectral data. No augmentation was applied to the validation set to ensure unbiased performance evaluation.

Fine-Tuning Strategy

A two-stage fine-tuning strategy was adopted:

Encoder Freezing (Warm-up Phase): During the first three epochs, the encoder weights were frozen to preserve previously learned low-level features while allowing the decoder and segmentation head to adapt to the new dataset (Dobrzycki et al., 2025).

Full Fine-Tuning: After the warm-up period, the encoder layers were unfrozen, and the entire network was trained end-to-end. This allowed deeper feature representations to gradually adjust to domain-specific differences, such as land cover appearance, illumination, and sensor characteristics.

Class Imbalance Recalibration

Due to the class distribution differences in the new dataset, the positive class weight for the BCEWithLogitsLoss function was recalculated using only the training split of the target dataset. The ratio of background to ASM pixels was computed and used to update the loss function, ensuring that the fine-tuning process remained sensitive to the minority class. To further stabilize fine-tuning and prevent large updates from disrupting pretrained features, differential learning rates were used:

Encoder learning rate: 1×10^{-5}

Decoder and segmentation head learning rate: 1×10^{-4}

This approach allowed the newly initialized decoder layers to learn more rapidly, while applying smaller, more conservative updates to the pretrained encoder (Konar et al., 2020; Xu et al., 2025).

Optimization and Learning Rate Scheduling

Training employed the Adam optimizer with parameter groups corresponding to the encoder and decoder components. A ReduceLROnPlateau scheduler monitored validation loss and reduced the learning rate by a factor of 0.5 if no improvement was observed for four consecutive epochs. This strategy enabled large optimization steps during early fine-tuning and progressively smaller refinements as convergence was approached.

2.10 Spatial Overlap Analysis

A spatial overlap analysis was conducted to evaluate how well predicted ASM areas aligned geographically with reference ASM data. This assessment goes beyond pixel-based accuracy metrics by measuring the practical spatial agreement between model outputs and true ASM distributions.

Full image prediction maps were generated using a sliding-window approach, where the trained U-Net model was applied to overlapping 256×256 pixel image patches. The resulting binary predictions were mosaicked into a seamless raster matching the original imagery's resolution and coordinate system.

Spatial overlap was then calculated as the proportion of predicted ASM pixels that coincided with reference ASM pixels. This analysis was performed for both the zero-shot transfer model and the fine-tuned model to quantify improvements in spatial consistency after fine-tuning.

3. RESULTS

3.1 MODEL COMPARISON

3.1.1 SEGMENTATION PERFORMANCE IN MADRE DE DIOS

Table 3.1 shows the performance of 4 segmentation models (M1–M4) that were trained and evaluated in the Madre de Dios region. The first model, M1, considered only the RGB Bands and the second, M2, considered the RGB Bands and three infrared bands (*NIR, SWIR1 and SWIR2*). The third model, M3, also considered the RGB Bands and three vegetative and water indices (*NDVI + EVI + MNDWI)*, and the last model, M4, considered the RGB Bands, the three infrared bands and the three spectral indices. The models demonstrated consistently strong performance across all feature combinations with an overall accuracy values ranging between approximately 0.96 and 0.97, while F1-scores exceeded 0.92 for all models. These results indicate a high level of agreement between predicted ASM areas and the reference labels.

Table 3.1 Quantitative performance of models in Madre de Dios.

Model	Accuracy	F1-Score	Precision	Recall	IoU
M1	0.962	0.926	0.916	0.937	0.870
M2	0.959	0.921	0.919	0.924	0.860
M3	0.965	0.933	0.936	0.931	0.880
M4	0.962	0.931	0.927	0.935	0.877

where

M1 = RGB Bands

M2 = RGB + NIR + SWIR1 + SWIR2

M3 = RGB + NDVI + EVI + MNDWI

M4 = RGB + NIR + SWIR1 + SWIR2 + RGB + NDVI + EVI + MNDWI

Among the evaluated models, the combinations incorporating RGB bands together with vegetation and water-related indices achieved the highest performance. This model recorded an F1-score of 0.933 and an IoU of 0.880, indicating superior spatial correspondence and boundary delineation of ASM features. Precision and recall values were well balanced, suggesting that both commission and omission errors were relatively limited in the source domain.

The high performance observed across all models confirms that ASM features in Madre de Dios exhibit distinct spectral and spatial characteristics that can be effectively captured using Sentinel-2 imagery and a segmentation-based DL approach.

3.2 Influence of Input Feature Combinations

Differences in model performance were observed across the various input feature combinations. The model, M1, relying solely on RGB bands achieved strong results, reflecting the clear visual contrast between ASM areas and surrounding forest cover in Madre de Dios. However, this model consistently exhibited slightly lower IoU values compared to models that incorporated additional spectral information.

The inclusion of vegetation indices (NDVI and EVI) and a water index (MNDWI) resulted in improved segmentation accuracy and spatial coherence. These indices enhanced the model's ability to distinguish mined areas from vegetation and natural water bodies.

The model that combined both spectral bands and indices showed slight improvements over RGB-only combinations, indicating that feature enrichment contributes to more precise spatial delineation rather than large gains in pixel-level accuracy. Overall, the results demonstrate that the choice of input features influences segmentation quality, particularly in terms of boundary definition and spatial consistency.

3.3 Zero-Shot Transfer Results in Kayapó

When the model trained in Madre de Dios was directly applied to the Kayapó region without any retraining, a noticeable decline in performance was observed. In the results presented in Table 3.2, the zero-shot transfer model achieved an F1-score of 0.763 and an IoU of 0.648, representing a substantial reduction relative to the model M3.

Table 3.2 Quantitative performance of zero-short transfer in Kayapó region, Brazil.

Region	Accuracy	F1-Score	Precision	Recall	IoU
Madre de Dios	0.965	0.933	0.936	0.931	0.880
Kayapo (ZS)	0.868	0.763	0.767	0.7645	0.648

where
ZS = Zero-shot

Despite this decrease, the zero-shot model successfully identified major ASM patterns, particularly those associated with riverine mining activities. Large and continuous mining features were generally detected, while smaller or more fragmented ASM areas were more frequently missed. Errors were also observed in areas characterized by exposed sediments, different spectral differences, in soil and heterogeneous land cover.

The spatial overlap between predicted ASM areas and reference data in the zero-shot scenario was limited, with an overlap rate of 51.66%. This result indicates that approximately half of the predicted ASM extent corresponded to reference mining areas in the target region.

3.4 Fine-Tuned Model Performance

Fine-tuning the pretrained model using a limited set of labeled samples from the Kayapó region led to a clear improvement in performance across all evaluated metrics. In Table 3.3, the fine-tuned model achieved an F1-score of 0.850 and an IoU of 0.749, substantially outperforming the zero-shot configuration with F1-score of 0.763 and an IoU of 0.648.

Table 3.3 Quantitative performance of Transfer Learning in Kayapó region, Brazil.

Region	Accuracy	F1-Score	Precision	Recall	IoU
Madre de Dios	0.965	0.933	0.936	0.931	0.880
Kayapo(ZS)	0.868	0.763	0.767	0.7645	0.648
Kayapo(FT)	0.9027	0.8495	0.8288	0.8780	0.749

where
ZS = Zero-shot
FT = Fine-tuned

Precision and recall increased to 0.8288 and 0.8780, respectively, indicating improved discrimination between mining and non-mining areas and enhanced detection of smaller and more fragmented ASM features.

Visual inspection of the full-image predictions confirms improved boundary alignment, reduced overestimation in non-mining areas, and increased continuity of detected ASM features compared to the zero-shot results.

3.5 Spatial Overlap Analysis

Figures 3.1 and 3.2 present the ASM reference maps used as labels, the predicted ASM maps, and the spatial overlap between the reference and predicted mining areas for zero-shot learning and fine-tuned TL, respectively. Figures 3.1a and 3.2a show the spatial distribution of ASM sites within the Kayapó study area derived from the Hansen Forest Cover Loss dataset. These areas represent deforestation resulting from ASM activities and are therefore considered ASM sites.

Figures 3.1b and 3.2b illustrate the areas predicted as ASM sites by the segmentation models using zero-shot learning and fine-tuned TL, respectively. Although some ASM sites were not correctly identified by the models, the predictions generally captured key spatial and spectral characteristics associated with ASM activities. The square patterns observed in the final predictions map (Figures 3.1b and 3.2b) are linked to the presence of masked pixels introduced during cloud masking process. Even though only a few pixels within the tile were masked, the model processes the image in spatial neighborhoods, meaning that these masked values may have affected predictions across the entire 256×256 patch. This likely contributed to the block-like artifacts seen in the reconstructed image in Figures 3.1b and 3.2b.

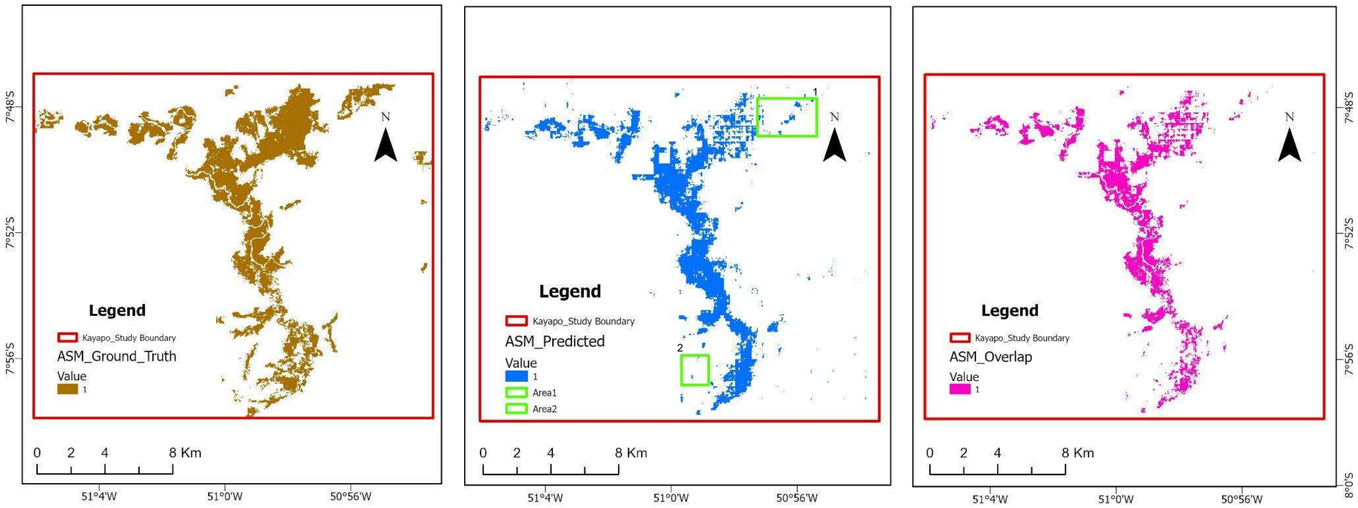

(a) (b) (c)

Figure 3.1 – Spatial Overlap of Zero-shot prediction and reference data in Kayapó

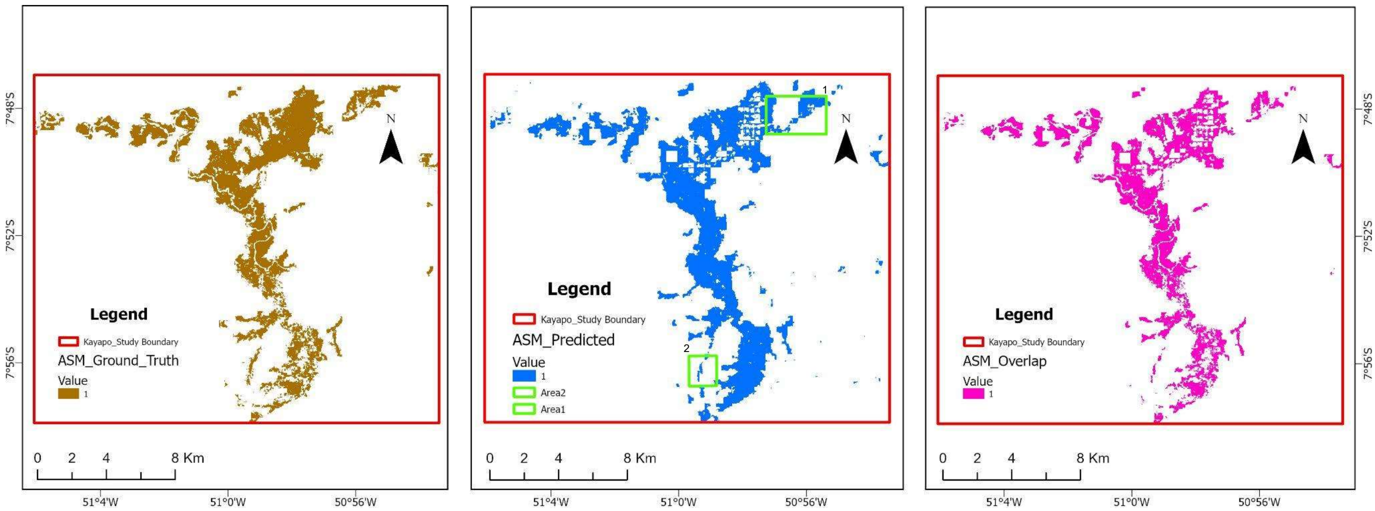

(a) (b) (c)

Figure 3.2 – Spatial Overlap of Fine-tuned prediction and reference data in Kayapó

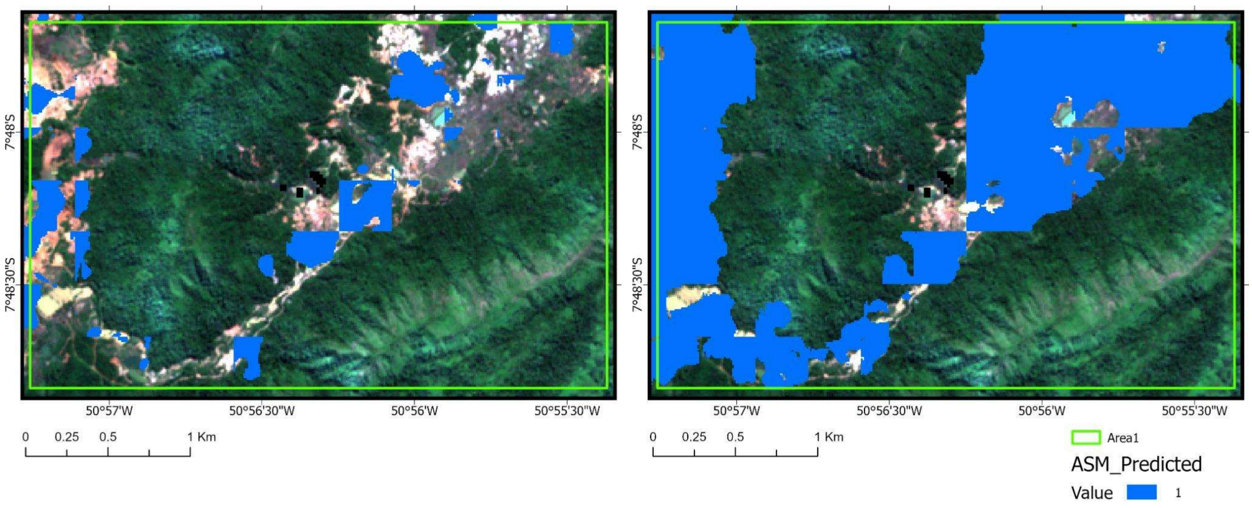

(a) (b)

Figure 3.3 – Zoomed in Area 1 of Figures 3.1b and 3.2b

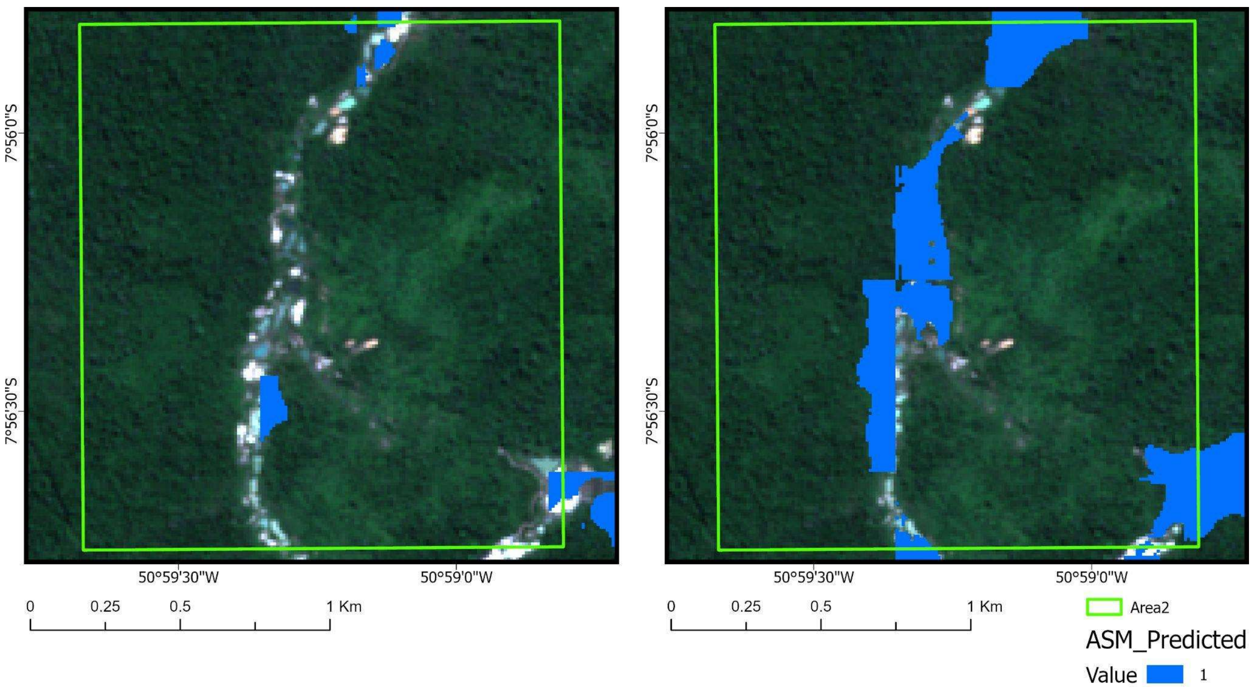

(a) (b)

Figure 3.4 – Zoomed in Area 2 of Figures 3.1b and 3.2b

Table 3.4 Spatial Overlap Results for zero-short and fine-tuned Transfer Learning in Kayapó region, Brazil.

Region	Overlap	TP	FP	FN	TN	Area(ha)
Kayapo (ZS)	51.66%	245016	98740	229277	4185717	2413.23
Kayapo (FT)	80.06%	379717	172782	94576	4111675	3739.93

where

ZS = Zero-shot

FT = Fine-tuned

Figures 3.1c and 3.2c depict the spatial overlap between the reference ASM areas (Figures 3.1a and 3.2a) and the predicted ASM areas (Figures 3.1b and 3.2b). This overlap represents the areas accurately classified as ASM by the models, corresponding to approximately 52% and 80% of the reference ASM areas for the zero-shot and fine-tuned models, respectively as shown in Table 3.4. This analysis demonstrates that fine-tuning enhances not only pixel-level classification accuracy but also improves the spatial consistency and geometric precision of ASM predictions, which are essential for effective environmental monitoring and impact assessment.

Spatial overlap analysis further highlights the differences between TL strategies. In the zero-shot scenario, the overlap between predicted and reference ASM areas was limited to 51.66%, indicating substantial spatial disagreement. After fine-tuning, spatial overlap increased markedly to 80.06%, reflecting improved alignment between predicted ASM extents and reference data. The fine-tuned model more accurately captured the shape, extent, and continuity of mining features, particularly along river corridors where ASM activity is concentrated. Figure 3.3a and Figure 3.3b shows maps of the same area of where the zero-shot and fine-tuned model was applied and depicts how the fine-tuning improved the prediction of the same area. Figure 3.4a and Figure 3.4b also shows maps of the same area of where the zero-shot and fine-tuned model was applied and depicts how fine-tuned model helped recover ASM site along smaller tributaries that were missed in during the direct model application.

4. DISCUSSION

4.1 Interpretation of Segmentation Results

The segmentation results obtained in the Madre de Dios region demonstrate that DL–based semantic segmentation is an effective approach for mapping ASM using Sentinel-2 imagery. The high F1-scores and IoU values reported in Table 3.1 indicate that the model was able to accurately distinguish mining areas from surrounding forest and river environments. This suggests that ASM activities in Madre de Dios produce strong and consistent spectral and spatial signatures that can be learned by convolutional neural networks.

The balanced precision and recall values observed in the source domain further indicate that the model achieved a good compromise between false positive and false negative detections. This balance is particularly important for environmental monitoring applications, where both overprediction and underprediction of disturbed areas can affect subsequent analysis and decision-making.

The segmentation results confirm that the adopted U-Net architecture, combined with appropriate input features, is suitable for ASM detection in tropical forest environments.

4.2 Effect of Spectral Indices on ASM Detection

All four model configurations achieved high performance metrics, indicating that segmentation-based DL is effective for ASM detection in Madre de Dios. However, differences in F1-score and IoU reveal the impact of feature selection on segmentation quality. The results in Table 3.1 show that model M3 incorporating spectral indices such as NDVI, EVI, and MNDWI outperformed those relying solely on RGB bands, particularly in terms of spatial delineation and boundary accuracy. These improvements can be attributed to the ability of vegetation indices to capture forest degradation and canopy loss, while water indices highlight sediment-rich mining ponds and disturbed river channels. This further supports the findings by Fonseca et al. (2024) and Madasa et al. (2021) that vegetation indices improve the performance in ASM delineation.

RGB bands (M1) provide strong visual contrast between mining areas and intact forest, spectral indices offer complementary information that improves discrimination in transition zones, such as riverbanks and partially revegetated areas. The observed increase in IoU for index-enhanced models suggests that these features are especially valuable for refining the spatial extent of ASM areas rather than substantially increasing pixel-level accuracy.

Even though Model M4 combined all spectral bands and indices, it did not outperform M3, suggesting that the inclusion of additional spectral information may introduce redundancy rather than improve feature separability (Fonseca et al., 2024). These results indicate the importance of targeted feature selection in ASM delineation and that it should always be considered instead of adding more bands or features, which may not be necessary and important. Based on the model with the best performance, M3 was selected as the source model for subsequent TL experiments.

The finding supports the importance of feature selection in segmentation-based remote sensing workflows and supports the inclusion of domain-relevant indices for environmental disturbance mapping.

4.3 Model Transferability and Generalization

When the model M3 was applied to the Kayapó region without retraining, the model exhibited reduced performance compared to the performance on the validation dataset from the Madre de Dios region. The F1-score decreased by approximately 18%, while IoU dropped from 0.880 to 0.648. This reduction reflects limited model generalization across regions with different environmental and geomorphological characteristics including differences in soil color and composition and variations in river width and morphology. Although both Madre de Dios and Kayapó are affected by ASM and located within the Amazon Basin, differences in river morphology, sediment properties, vegetation structure, and mining practices influenced the spectral and spatial patterns captured by Sentinel-2 imagery for instance in Madre de Dios, mining area were characterised by milky or chalky clay soil but there were some mining areas in Kayapó that had reddish clay and dark soil

which could be abandoned sites as shown in Figure 3.3 and these couldn't be detected by the model.
Despite these differences, the zero-shot transfer results demonstrate that the model retained the ability to detect large and certain spatial patterns learned in the source domain are transferable, even in the continuous ASM features in areas where mining sites are clustered more. This shows the presence of regional variability. However, smaller and more fragmented mining areas were more frequently missed, and confusion with natural sediment features increased.

The results for the spatial overlap analysis (Table 3.4) also reveal, the zero-shot model correctly identified 245,016 ASM pixels (true positives), but failed to detect a substantial number of reference ASM pixels, resulting in 229,277 false negatives. This high false-negative count indicates that many ASM areas were omitted, particularly smaller or fragmented mining sites. Additionally, the model produced 98,740 false positives, reflecting confusion between ASM and spectrally similar land-cover types such as exposed soils and riverine sediments.

The spatial overlap between predicted ASM areas and reference data in the zero-shot scenario was limited, with an overlap rate of 51.66% indicating that approximately half of the predicted ASM extent corresponded to reference mining areas in the Kayapó, suggesting that while direct model transfer can provide useful preliminary information, it is insufficient for accurate and reliable ASM mapping in new regions.

4.4 Effectiveness of Transfer Learning

Fine-tuning the pretrained model, M3, using a limited set of labeled samples from the Kayapó region resulted in substantial improvements across all evaluation metrics (Table 3.3). The fine-tuned model achieved an F1-score of 0.8495 and an IoU of 0.749, representing significant gains over the zero-shot configuration. The increase in F1-score, IoU, and spatial overlap demonstrates that TL effectively mitigated the performance loss observed in the zero-shot scenario.

Precision and recall increased to 0.8288 and 0.8780, respectively, indicating improved discrimination between mining and non-mining areas and enhanced detection of smaller and more fragmented ASM features. The most notable improvement was observed in recall, indicating that fine-tuning enabled the model to better detect ASM areas that were previously omitted, mostly mining pits along small tributaries. This improvement is particularly important for monitoring illegal mining, where missed detections may allow continued environmental degradation. The concurrent improvement in precision suggests that fine-tuning also helped the model reduce false positives by adapting to region-specific spectral characteristics.

The confusion matrix (Table 3.4) further highlights the impact of fine-tuning. The number of true positives increased markedly from 245,016 to 379,717 pixels, while false negatives were reduced from 229,277 to 94,576 pixels. This reduction in false negatives demonstrates that fine-tuning enabled the model to better capture smaller and more fragmented ASM sites that were previously missed. Although the number of false positives increased to 172,782 pixels, this was partly due to the heterogeneous structure of mining landscapes, where vegetation patches and river channels occur within or adjacent to excavation zones. The model's reliance on spatial context led to the inclusion of these neighbouring features within predicted mining areas. Also, this reflects a more inclusive detection strategy that prioritized capturing ASM extent, which is often preferable in environmental monitoring applications.

The estimated ASM area also increased substantially from 2413.23 hectares to 3,739.93 hectares following fine-tuning. This increase suggests that the zero-shot model systematically underestimated ASM extent, whereas the fine-tuned model produced a more comprehensive representation of mining activity in the region. Visual inspection of the fine-tuned predictions confirmed these quantitative findings, showing improved boundary delineation, greater spatial continuity, and enhanced detection of dispersed ASM features.

The spatial overlap with reference data (Figure 3.2a; Figure 3.2b) increased markedly to 80.06%, confirming improved geometric agreement and boundary delineation. These results demonstrate that TL effectively mitigates the limitations of zero-shot transfer by enabling the model to adapt to region-specific spectral and spatial characteristics using minimal annotation effort. Transfer learning is an effective way for adapting segmentation models to new geographic regions while minimizing the need for extensive local training data.

4.5 Comparison with Previous Studies

The findings of this study are consistent with previous research that has demonstrated the effectiveness of DL methods for mining and deforestation detection using optical satellite imagery. Earlier studies have shown that ASM activities generate distinct spatial and spectral signatures, particularly in riverine environments, which can be captured using medium- to high-resolution RS data (Becerra et al., 2024; Gallwey et al., 2020; Nursamsi et al., 2024).

Compared to traditional classification approaches, the segmentation-based method used in this study provides more detailed spatial representations of mining extents, allowing for improved boundary delineation(Gallwey et al., 2020; Simionato et al., 2021). The observed performance improvements achieved through TL also align with existing literature on domain adaptation in RS, which highlights the challenges of cross-regional generalization and the benefits of fine-tuning pretrained models (Dastour & Hassan, 2023; Y. Ma et al., 2024). By directly comparing zero-shot and fine-tuned transfer strategies, this study contributes empirical evidence on the practical limits and advantages of TL for ASM detection.

4.6 Implications for ASM Monitoring and Policy

The results of this study have important implications for large-scale ASM monitoring and environmental policy. The ability to train a model in one region and adapt it to another using limited additional data supports the development of scalable monitoring systems for remote and data-scarce areas. This is particularly relevant for indigenous territories and protected areas, where extensive field data collection may be difficult or restricted.

From a policy perspective, the proposed approach can support early detection of illegal mining activities, improve the allocation of enforcement resources, and contribute to more timely environmental impact assessments. The use of freely available Sentinel-2 imagery further enhances the accessibility and cost-effectiveness of the method for governmental and non-governmental organizations.

4.7 Study Limitations

Despite the promising results, several limitations should be acknowledged. First, the reliance on optical Sentinel-2 imagery makes the approach sensitive to cloud cover and seasonal variability, which can reduce data availability and affect model performance. Second, the spatial resolution of Sentinel-2 limits the detection of very small or early-stage ASM sites.

Additionally, the quality of reference data, Hansen Global Forest Change (GFC) dataset may influence performance evaluation, particularly in rapidly changing mining environments. The dataset is derived from 30m Landsat imagery, which may not capture small-scale or early-stage ASM activities. Finally, the study focused on a single study area (Kayapo) for transfer-learning, and further validation across additional geographic contexts would be required to fully assess model generalization as different regions may have different ways of mining and how the way of mining influences the spatial distribution of the mining areas.

5. CONCLUSION

This study demonstrates the effectiveness of segmentation-based deep learning (DL) combined with transfer learning (TL) for detecting and delineating artisanal and small-scale mining (ASM) activities using Sentinel-2 imagery in tropical environments. Using Madre de Dios, Peru, as the source region, the study evaluated model performance within the training region and examined its transferability to the geographically distinct Kayapó region in Brazil.

The findings confirm that a segmentation-based U-Net model trained on Sentinel-2 imagery can effectively detect and delineate ASM in Madre de Dios, thereby addressing the first research question "How effectively can a segmentation-based deep learning model trained on Sentinel-2 imagery detect and delineate ASM in Madre de Dios, Peru?". The models demonstrated consistently strong performance across all feature combinations, with overall accuracy ranging between 0.96 and 0.97 and F1-scores exceeding 0.92. The best-performing configuration achieved an F1-score of 0.933 and an IoU of 0.880, indicating high spatial correspondence and accurate boundary delineation of ASM features. The integration of spectral indices (NDVI, EVI, and MNDWI) with RGB bands significantly enhanced segmentation performance, underscoring the importance of vegetation- and water-sensitive features in distinguishing mining disturbances from surrounding land cover.

However, direct transfer of the trained model to Kayapó without retraining resulted in a substantial decline in performance, thus answering the second research question "To what extent can the Madre de Dios model be transferred to Kayapó without retraining (direct model transfer)?". The zero-shot transfer model achieved an F1-score of 0.763 and an IoU of 0.648, representing a marked reduction relative to the source-region model. Spatial agreement was also limited, with an overlap rate of 51.66% between predicted and reference ASM areas. These results highlight the sensitivity of deep learning models to domain shift and regional environmental variability, demonstrating that direct cross-regional generalization is constrained without adaptation.

In contrast, fine-tuning the pretrained model with a limited set of labeled samples from Kayapó significantly improved performance, directly addressing the third research question "How does transfer learning (fine-tuning) improve ASM segmentation detection performance in Kayapó compared to direct model transfer?". The fine-tuned model achieved an F1-score of 0.850 and an IoU of 0.749, substantially outperforming the zero-shot configuration. Spatial overlap increased from 51.66% to 80.06%, indicating markedly improved geometric alignment and spatial consistency of ASM predictions. These results demonstrate that transfer learning effectively adapts pretrained spatial representations to new environmental conditions while requiring relatively minimal additional annotation effort.

Overall, this study establishes that while segmentation-based DL models achieve high accuracy within a trained region, their cross-regional applicability depends on appropriate adaptation strategies. Transfer learning provides a practical and data-efficient solution for extending ASM monitoring frameworks to new geographic contexts. The proposed approach contributes to the development of scalable remote sensing methodologies capable of supporting environmental monitoring, regulatory enforcement, and sustainable land management in tropical regions.

5.1 FUTURE WORKS

Although this study demonstrates the effectiveness of segmentation-based DL and TL for ASM detection, several areas remain for further improvement. Future research should explore the integration of multi-sensor data, particularly combining Sentinel-2 optical imagery with Sentinel-1 SAR data, to improve detection under cloudy conditions and enhance discrimination of mining features. The use of higher-resolution imagery could also support better identification of small or early-stage mining sites and improve boundary delineation.

Improving reference datasets is another important direction, as forest loss data do not exclusively represent mining activities. Developing ASM-specific ground truth through high-resolution imagery interpretation or field validation would strengthen model training and evaluation. Also, the areas considered in this study were mostly forested areas affected by ASM making the classification between ASM sites and non-ASM sites. Studies should consider multiclass delineation to see how segmentation based ASM models can distinguish between different classes like ASM affected areas, urban areas, forests, farmland and waterbodies. Advanced domain adaptation techniques could further enhance cross-regional model transferability while reducing reliance on large labeled datasets.

Future work should also consider extending the approach to spatio-temporal monitoring to track the evolution of ASM activities over time. Expanding the framework to additional geographic regions and incorporating explainable AI methods would improve model robustness and transparency. Ultimately, implementing this approach within an operational, cloud-based monitoring system could support near-real-time detection of mining activities and inform environmental management and policy decisions.

BIBLIOGRAPHY

Akpah, S., Ziggah, Y. Y., & Mireku-Gyimah, D. (2022). Assessing the suitability of convolutional auto encoder as an unsupervised tool for image classification in artisanal small-scale gold mining environment. *International Journal of Computing and Artificial Intelligence*, *3*(1), 26–40. https://doi.org/10.33545/27076571.2022.v3.i1a.43

Alessi, M. A., Chirico, P. G., Sunder, S., & O'Pry, K. L. (2023). Detection and Monitoring of Small-Scale Diamond and Gold Mining Dredges Using Synthetic Aperture Radar on the Kadéï (Sangha) River, Central African Republic. *Remote Sensing*, *15*(4), 913. https://doi.org/10.3390/rs15040913

Ashe, K. (2012). Elevated Mercury Concentrations in Humans of Madre de Dios, Peru. *PLoS ONE*, *7*(3), e33305. https://doi.org/10.1371/journal.pone.0033305

Asner, G. P., Llactayo, W., Tupayachi, R., & Luna, E. R. (2013). Elevated rates of gold mining in the Amazon revealed through high-resolution monitoring. *Proceedings of the National Academy of Sciences*, *110*(46), 18454–18459. https://doi.org/10.1073/pnas.1318271110

Asner, G. P., Powell, G. V. N., Mascaro, J., Knapp, D. E., Clark, J. K., Jacobson, J., Kennedy-Bowdoin, T., Balaji, A., Paez-Acosta, G., Victoria, E., Secada, L., Valqui, M., & Hughes, R. F. (2010). High-resolution forest carbon stocks and emissions in the Amazon. *Proceedings of the National Academy of Sciences*, *107*(38), 16738–16742. https://doi.org/10.1073/pnas.1004875107

Asner, G. P., & Tupayachi, R. (2016). Accelerated losses of protected forests from gold mining in the Peruvian Amazon. *Environmental Research Letters*, *12*(9), 094004. https://doi.org/10.1088/1748-9326/aa7dab

Basu, N., Renne, E., & Long, R. (2015). An Integrated Assessment Approach to Address Artisanal and Small-Scale Gold Mining in Ghana. *International Journal of Environmental Research and Public Health*, *12*(9), 11683–11698. https://doi.org/10.3390/ijerph120911683

Becerra, M., Villa, L., Nicolau, A. P., Herndon, K. E., Novoa, S., Martín-Arias, V., Dyson, K., Walker, K., Tenneson, K., & Saah, D. (2024). Creating near real-time alerts of illegal gold mining in the Peruvian Amazon using Synthetic Aperture Radar. *Environmental Research Communications*, *6*(12), 125022. https://doi.org/10.1088/2515-7620/ad937e

Caballero Espejo, J., Messinger, M., Román-Dañobeytia, F., Ascorra, C., Fernandez, L., & Silman, M. (2018). Deforestation and Forest Degradation Due to Gold Mining in the Peruvian Amazon: A 34-Year Perspective. *Remote Sensing*, *10*(12), 1903. https://doi.org/10.3390/rs10121903

Camalan, S., Cui, K., Pauca, V. P., Alqahtani, S., Silman, M., Chan, R., Plemmons, R. J., Dethier, E. N., Fernandez, L. E., & Lutz, D. A. (2022). Change Detection of Amazonian Alluvial Gold Mining Using Deep Learning and Sentinel-2 Imagery. *Remote Sensing*, *14*(7), 1746. https://doi.org/10.3390/rs14071746

Castro, M. C., Arisco, N. J., Diniz, C. G., Ponmattam, J., Peterka, C., Basta, P. C., & Ferreira, M. U. (2025). Mining and malaria in the Brazilian Amazon and in the Yanomami indigenous land. *PLOS Neglected Tropical Diseases*, *19*(11), e0013677. https://doi.org/10.1371/journal.pntd.0013677

Couttenier, M., Di Rollo, S., Inguere, L., Mohand, M., & Schmidt, L. (2022). Mapping artisanal and small-scale mines at large scale from space with deep learning. *PLOS ONE*, *17*(9), e0267963. https://doi.org/10.1371/journal.pone.0267963

Cui, K., Camalan, S., Li, R., Pauca, V. P., Alqahtani, S., Plemmons, R. J., Silman, M., Dethier, E. N., Lutz, D., & Chan, R. H. (2022). *Semi-supervised Change Detection of Small Water Bodies Using RGB and Multispectral Images in Peruvian Rainforests* (arXiv:2206.09365). arXiv. https://doi.org/10.48550/arXiv.2206.09365

da Silva, C. F. A., de Andrade, M. O., dos Santos, A. M., Falcão, V. A., & Martins, S. F. S. (2023). The drivers of illegal mining on Indigenous Lands in the Brazilian Amazon. *The Extractive Industries and Society*, *16*, 101354. https://doi.org/10.1016/j.exis.2023.101354

Daroya, R., Rowley, T., Flores, J., Friedmann, E., Bennitt, F., An, H., Simmons, T., Hughes, M. J., Kluetmeier, C. L., Kica, S., Vélez, J. D., Esenther, S. E., Howard, T. E., Ye, Y., Turcotte, A., Gleason, C., & Maji, S. (2025). *RiverScope: High-Resolution River Masking Dataset* (arXiv:2509.02451). arXiv. https://doi.org/10.48550/arXiv.2509.02451

Dastour, H., & Hassan, Q. K. (2023). A Comparison of Deep Transfer Learning Methods for Land Use and Land Cover Classification. *Sustainability*, *15*(10). https://doi.org/10.3390/su15107854

de Moura, N. V. A., de Carvalho, O. L. F., Gomes, R. A. T., Guimarães, R. F., & de Carvalho Júnior, O. A. (2022). Deep-water oil-spill monitoring and recurrence analysis in the Brazilian territory using Sentinel-1 time series and deep learning. *International Journal of Applied Earth Observation and Geoinformation*, *107*, 102695. https://doi.org/10.1016/j.jag.2022.102695

Dethier, E. N., Silman, M., Leiva, J. D., Alqahtani, S., Fernandez, L. E., Pauca, P., Çamalan, S., Tomhave, P., Magilligan, F. J., Renshaw, C. E., & Lutz, D. A. (2023). A global rise in alluvial mining increases sediment load in tropical rivers. *Nature*, *620*(7975), 787–793. https://doi.org/10.1038/s41586-023-06309-9

Dethier, E. N., Silman, M. R., Fernandez, L. E., Espejo, J. C., Alqahtani, S., Pauca, P., & Lutz, D. A. (2023). Operation mercury: Impacts of national-level armed forces intervention and anticorruption strategy on artisanal gold mining and water quality in the Peruvian Amazon. *Conservation Letters*, *16*(5), e12978. https://doi.org/10.1111/conl.12978

Diringer, S. E., Berky, A. J., Marani, M., Ortiz, E. J., Karatum, O., Plata, D. L., Pan, W. K., & Hsu-Kim, H. (2020). Deforestation Due to Artisanal and Small-Scale Gold Mining Exacerbates Soil and Mercury Mobilization in Madre de Dios, Peru. *Environmental Science & Technology*, *54*(1), 286–296. https://doi.org/10.1021/acs.est.9b06620

Diringer, S. E., Feingold, B. J., Ortiz, E. J., Gallis, J. A., Araújo-Flores, J. M., Berky, A., Pan, W. K. Y., & Hsu-Kim, H. (2015). River transport of mercury from artisanal and small-scale gold mining and risks for dietary mercury exposure in Madre de Dios, Peru. *Environmental Science: Processes & Impacts*, *17*(2), 478–487. https://doi.org/10.1039/C4EM00567H

Dobrzycki, A. D., Bernardos, A. M., & Casar, J. R. (2025). An Analysis of Layer-Freezing Strategies for Enhanced Transfer Learning in YOLO Architectures. *Mathematics*, *13*(15), 2539. https://doi.org/10.3390/math13152539

Dong, X., Li, J., Chang, Q., Miao, S., & Wan, H. (2025). Data Fusion and Models Integration for Enhanced Semantic Segmentation in Remote Sensing. *IEEE Journal of Selected Topics in Applied Earth Observations and Remote Sensing*, *18*, 7134–7151. https://doi.org/10.1109/JSTARS.2025.3528650

Drusch, M., Del Bello, U., Carlier, S., Colin, O., Fernandez, V., Gascon, F., Hoersch, B., Isola, C., Laberinti, P., Martimort, P., Meygret, A., Spoto, F., Sy, O., Marchese, F., & Bargellini, P. (2012). Sentinel-2: ESA's Optical High-Resolution Mission for GMES Operational Services. *Remote Sensing of Environment*, *120*, 25–36. https://doi.org/10.1016/j.rse.2011.11.026

Ej Atlas. (2023, July 18). *Ej Atlas, Ilegal mining in indigenous territories Kayapó, Pará, Brazil*. https://ejatlas.org/print/illegal-goldmining-kayapo-brazil

Elmes, A., Yarlequé Ipanaqué, J. G., Rogan, J., Cuba, N., & Bebbington, A. (2014). Mapping licit and illicit mining activity in the Madre de Dios region of Peru. *Remote Sensing Letters*, *5*(10), 882–891. https://doi.org/10.1080/2150704X.2014.973080

Fonseca, A., Marshall, M. T., & Salama, S. (2024). Enhanced Detection of Artisanal Small-Scale Mining with Spectral and Textural Segmentation of Landsat Time Series. *Remote Sensing*, *16*(10), 1749. https://doi.org/10.3390/rs16101749

Fritz, W. M., McQuilken, J., Collins, N., & Weldegiorgis, F. (2014). *Global Trends in Artisanal and Small-Scale Mining (ASM): A review of key numbers and issues*. https://www.iisd.org/system/files/publications/igf-asm-global-trends.pdf

Gallwey, J., Robiati, C., Coggan, J., Vogt, D., & Eyre, M. (2020). A Sentinel-2 based multispectral convolutional neural network for detecting artisanal small-scale mining in Ghana: Applying deep learning to shallow mining. *Remote Sensing of Environment*, *248*, 111970. https://doi.org/10.1016/j.rse.2020.111970

Gerson, J. R., Szponar, N., Zambrano, A. A., Bergquist, B., Broadbent, E., Driscoll, C. T., Erkenswick, G., Evers, D. C., Fernandez, L. E., Hsu-Kim, H., Inga, G., Lansdale, K. N., Marchese, M. J., Martinez, A., Moore, C., Pan, W. K., Purizaca, R. P., Sánchez, V., Silman, M., … Bernhardt, E. S. (2022). Amazon forests capture high levels of atmospheric mercury pollution from artisanal gold mining. *Nature Communications*, *13*(1), 559. https://doi.org/10.1038/s41467-022-27997-3

Giang, T. L., Dang, K. B., Toan Le, Q., Nguyen, V. G., Tong, S. S., & Pham, V.-M. (2020). U-Net Convolutional Networks for Mining Land Cover Classification Based on High-Resolution UAV Imagery. *IEEE Access*, *8*, 186257–186273. https://doi.org/10.1109/ACCESS.2020.3030112

Hansen, M. C., Potapov, P. V., Moore, R., Hancher, M., Turubanova, S. A., Tyukavina, A., Thau, D., Stehman, S. V., Goetz, S. J., Loveland, T. R., Kommareddy, A., Egorov, A., Chini, L., Justice, C.

O., & Townshend, J. R. G. (2013). High-Resolution Global Maps of 21st-Century Forest Cover Change. *Science*, *342*(6160), 850–853. https://doi.org/10.1126/science.1244693

Hejmanowska, B., Michałowska, K., Kramarczyk, P., & Głowienka, E. (2025). The Potential of U-Net in Detecting Mining Activity: Accuracy Assessment Against GEE Classifiers. *Applied Sciences*, *15*(17). https://doi.org/10.3390/app15179785

Hong, F., He, G., Wang, G., Zhang, Z., & Peng, Y. (2025). AuxTransUNet: Enhancing Remote Sensing Image Segmentation of Open-Pit Mining Areas in Qinghai–Tibet Plateau. *IEEE Journal of Selected Topics in Applied Earth Observations and Remote Sensing*, *18*, 20348–20358. https://doi.org/10.1109/JSTARS.2025.3595592

Iakubovskii, P. (2019). *GitHub—Qubvel-org/segmentation_models.pytorch: Semantic segmentation models with 500+ pretrained convolutional and transformer-based backbones.* GitHub. https://github.com/qubvel-org/segmentation_models.pytorch

IUCN NL. (2024, December 24). Gold mining in Madre de Dios: Mercury in every body | IUCN NL. https://www.iucn.nl/en/story/gold-mining-in-madre-de-dios-mercury-in-every-body/

Jiang, C., Abdul Halin, A., Yang, B., Abdullah, L. N., Manshor, N., & Perumal, T. (2024). Res-UNet Ensemble Learning for Semantic Segmentation of Mineral Optical Microscopy Images. *Minerals*, *14*(12), 1281. https://doi.org/10.3390/min14121281

Kimijima, S., Sakakibara, M., & Nagai, M. (2021). Detection of Artisanal and Small-Scale Gold Mining Activities and Their Transformation Using Earth Observation, Nighttime Light, and Precipitation Data. *International Journal of Environmental Research and Public Health*, *18*(20), 10954. https://doi.org/10.3390/ijerph182010954

Kingma, D. P., & Ba, J. (2017). *Adam: A Method for Stochastic Optimization* (arXiv:1412.6980). arXiv. https://doi.org/10.48550/arXiv.1412.6980

Konar, J., Khandelwal, P., & Tripathi, R. (2020). Comparison of Various Learning Rate Scheduling Techniques on Convolutional Neural Network. *2020 IEEE International Students' Conference on Electrical,Electronics and Computer Science (SCEECS)*, 1–5. https://doi.org/10.1109/SCEECS48394.2020.94

Kopec, E., Wijata, A. M., & Nalepa, J. (2025). Change detection in Sentinel-2 images using deep learning ensembles. *Remote Sensing Applications: Society and Environment*, *40*, 101764. https://doi.org/10.1016/j.rsase.2025.101764

Kupcikevicius, I., Boretto, L., Grunbeck, I. A., Kumar, R. P., Nainamalai, V., Akhavi, M. S., Edwin, B., & Elle, O. J. (2025, November 5). *AI-Enabled Vessels Segmentation Model for Real-Time Laparoscopic Ultrasound Imaging*. Northern Lights Deep Learning Conference 2026. https://openreview.net/forum?id=TGk5TQNh18#discussion

Kwang, C., Afele, I. K., Yeboah, E., Sarfo, I., Batame, M., Okrah, A., Shwe, M. M., Siaw, W., Boyetey, D., Larbi, R. O., Mensah, A. O. K. N., El Rhadiouini, C., Jaffry, A. H., Siddique, F., Aftab, R., & Isinkaralar, O. (2025). Machine learning assessment of illegal mining (Galamsey) impacts on forest vegetation: A case study of Wassa Amenfi East District, Ghana. *Earth Science Informatics*, *18*(2), 348. https://doi.org/10.1007/s12145-025-01860-7

Li, W., Wang, Z., Wang, Y., Wu, J., Wang, J., Jia, Y., & Gui, G. (2020). Classification of High-Spatial-Resolution Remote Sensing Scenes Method Using Transfer Learning and Deep Convolutional Neural Network. *IEEE Journal of Selected Topics in Applied Earth Observations and Remote Sensing*, *13*, 1986–1995. https://doi.org/10.1109/JSTARS.2020.2988477

Luethje, F., Kranz, O., & Schoepfer, E. (2014). Geographic Object-Based Image Analysis Using Optical Satellite Imagery and GIS Data for the Detection of Mining Sites in the Democratic Republic of the Congo. *Remote Sensing*, *6*(7), 6636–6661. https://doi.org/10.3390/rs6076636

Ma, L., Liu, Y., Zhang, X., Ye, Y., Yin, G., & Johnson, B. A. (2019). Deep learning in remote sensing applications: A meta-analysis and review. *ISPRS Journal of Photogrammetry and Remote Sensing*, *152*, 166–177. https://doi.org/10.1016/j.isprsjprs.2019.04.015

Ma, Y., Chen, S., Ermon, S., & Lobell, D. B. (2024). Transfer learning in environmental remote sensing. *Remote Sensing of Environment*, *301*, 113924. https://doi.org/10.1016/j.rse.2023.113924

Madasa, A., Orimoloye, I. R., & Ololade, O. O. (2021). Application of geospatial indices for mapping land cover/use change detection in a mining area. *Journal of African Earth Sciences*, *175*, 104108. https://doi.org/10.1016/j.jafrearsci.2021.104108

Markham, K. E., & Sangermano, F. (2018). Evaluating Wildlife Vulnerability to Mercury Pollution From Artisanal and Small-Scale Gold Mining in Madre de Dios, Peru. *Tropical Conservation Science*, *11*, 1940082918794320. https://doi.org/10.1177/1940082918794320

Mataveli, G., Chaves, M., Guerrero, J., Escobar-Silva, E. V., Conceição, K., & De Oliveira, G. (2022). Mining Is a Growing Threat within Indigenous Lands of the Brazilian Amazon. *Remote Sensing*, *14*(16), 4092. https://doi.org/10.3390/rs14164092

Nava, L., Cuevas, M., Meena, S. R., Catani, F., & Monserrat, O. (2022). Artisanal and Small-Scale Mine Detection in Semi-Desertic Areas by Improved U-Net. *IEEE Geoscience and Remote Sensing Letters*, *19*, 1–5. https://doi.org/10.1109/LGRS.2022.3220487

Ngom, N. M., Baratoux, D., Bolay, M., Dessertine, A., Abass Saley, A., Baratoux, L., Mbaye, M., Faye, G., Yao, A. K., & Kouamé, K. J. (2023). Artisanal Exploitation of Mineral Resources: Remote Sensing Observations of Environmental Consequences, Social and Ethical Aspects. *Surveys in Geophysics*, *44*(1), 225–247. https://doi.org/10.1007/s10712-022-09740-1

Ngom, N. M., Mbaye, M., Baratoux, D., Baratoux, L., Catry, T., Dessay, N., Faye, G., Sow, E. H., & Delaitre, E. (2020). Mapping Artisanal and Small-Scale Gold Mining in Senegal Using Sentinel 2 Data. *GeoHealth*, *4*(12), e2020GH000310. https://doi.org/10.1029/2020GH000310

Nicolau, A. P., Herndon, K., Flores-Anderson, A., & Griffin, R. (2019). A spatial pattern analysis of forest loss in the Madre de Dios region, Peru. *Environmental Research Letters*, *14*(12), 124045. https://doi.org/10.1088/1748-9326/ab57c3

Nugroho, U. C., Susantoro, T. M., Kushardono, D., Nugroho, G., Setiawan, H. L., Suliantara, & Ichsan, N. (2024). Semantic Deep Learning for Open-Pit Mining Detection Using High Resolution SAR Data. *2024 IEEE International Conference on Aerospace Electronics and Remote Sensing Technology (ICARES)*, 1–6. https://doi.org/10.1109/ICARES64249.2024.10768071

Nursamsi, I., Phinn, S. R., Levin, N., Luskin, M. S., & Sonter, L. J. (2024). Remote sensing of artisanal and small-scale mining: A review of scalable mapping approaches. *Science of The Total Environment*, *951*, 175761. https://doi.org/10.1016/j.scitotenv.2024.175761

Nyamekye, C., Ghansah, B., Agyapong, E., & Kwofie, S. (2021). Mapping changes in artisanal and small-scale mining (ASM) landscape using machine and deep learning algorithms. - A proxy evaluation of the 2017 ban on ASM in Ghana. *Environmental Challenges*, *3*, 100053. https://doi.org/10.1016/j.envc.2021.100053

Ofori-Ampofo, S., Zappacosta, A., Kuzu, R. S., Schauer, P., Willberg, M., & Zhu, X. X. (2025). SmallMinesDS: A Multimodal Dataset for Mapping Artisanal and Small-Scale Gold Mines. *IEEE Geoscience and Remote Sensing Letters*, *22*, 1–5. https://doi.org/10.1109/LGRS.2025.3566356

Owusu-Nimo, F., Mantey, J., Nyarko, K. B., Appiah-Effah, E., & Aubynn, A. (2018). Spatial distribution patterns of illegal artisanal small scale gold mining (Galamsey) operations in Ghana: A focus on the Western Region. *Heliyon*, *4*(2), e00534. https://doi.org/10.1016/j.heliyon.2018.e00534

Pasanisi, F., Masolele, R. N., & Reiche, J. (2025). Using High-Resolution Satellite Imagery and Deep Learning to Map Artisanal Mining Spatial Extent in the Democratic Republic of the Congo. *Remote Sensing*, *17*(24), 4057. https://doi.org/10.3390/rs17244057

Peña-Villacreses, G., Ayala-Hidalgo, S., Braga, D., Guimarães, Y., Santos, M. R. D. S., Pereira, M. D. A., & Velastegui-Montoya, A. (2024). Trends of Remote Sensing applications for Amazon monitoring. *The International Archives of the Photogrammetry, Remote Sensing and Spatial Information Sciences*, *XLVIII-3–2024*, 393–399. https://isprs-archives.copernicus.org/articles/XLVIII-3-2024/393/2024/

Perez-Guerra, J., Herrera-Ruiz, V., Gonzalez-Velez, J. C., Martinez-Vargas, J. D., & Torres-Madronero, M. C. (2024). Land Cover Classification Using Remote Sensing and Supervised Convolutional Neural Networks. In M. Tabares, P. Vallejo, B. Suarez, M. Suarez, O. Ruiz, & J. Aguilar (Eds.), *Advances in Computing* (pp. 13–24). Springer Nature Switzerland. https://link.springer.com/chapter/10.1007/978-3-031-47372-2_2

Pires De Lima, R., & Marfurt, K. (2019). Convolutional Neural Network for Remote-Sensing Scene Classification: Transfer Learning Analysis. *Remote Sensing*, *12*(1), 86. https://doi.org/10.3390/rs12010086

Rjc, C., Lmv, N., Ila, R., Egr, A., Cml, C., & Lnm, T. (2023). Rev Gaúcha Enferm. *Rev Gaúcha Enferm.* https://www.scielo.br/j/rgenf/a/VnhpFLmYFz3TgCyKW8c5QRz/?format=pdf&lang=en

Ronneberger, O., Fischer, P., & Brox, T. (2015). *U-Net: Convolutional Networks for Biomedical Image Segmentation* (arXiv:1505.04597). arXiv. https://doi.org/10.48550/arXiv.1505.04597

Rorato, A. C., Camara, G., Escada, M. I. S., Picoli, M. C. A., Moreira, T., & Verstegen, J. A. (2020). Brazilian amazon indigenous peoples threatened by mining bill. *Environmental Research Letters*, *15*(10), 1040a3. https://doi.org/10.1088/1748-9326/abb428

Saka, U. M., Pacheco-Hague, K., Duzgun, S., & Smith, N. (2024). An analysis of the impact of CO2 emissions from deforestation and mining in Madre de Dios, Perú. *The Extractive Industries and Society*, *20*, 101526. https://doi.org/10.1016/j.exis.2024.101526

Saputra, M. R. U., Bhaswara, I. D., Nasution, B. I., Ern, M. A. L., Husna, N. L. R., Witra, T., Feliren, V., Owen, J. R., Kemp, D., & Lechner, A. M. (2025). Multi-modal deep learning approaches to semantic segmentation of mining footprints with multispectral satellite imagery. *Remote Sensing of Environment*, *318*, 114584. https://doi.org/10.1016/j.rse.2024.114584

Seccatore, J., Veiga, M., Origliasso, C., Marin, T., & De Tomi, G. (2014). An estimation of the artisanal small-scale production of gold in the world. *Science of The Total Environment*, *496*, 662–667. https://doi.org/10.1016/j.scitotenv.2014.05.003

Simionato, J., Bertani, G., & Osako, L. S. (2021). Identification of artisanal mining sites in the Amazon Rainforest using Geographic Object-Based Image Analysis (GEOBIA) and Data Mining techniques. *Remote Sensing Applications: Society and Environment*, *24*, 100633. https://doi.org/10.1016/j.rsase.2021.100633

Snapir, B., Simms, D. M., & Waine, T. W. (2017). Mapping the expansion of galamsey gold mines in the cocoa growing area of Ghana using optical remote sensing. *International Journal of Applied Earth Observation and Geoinformation*, *58*, 225–233. https://doi.org/10.1016/j.jag.2017.02.009

Sonter, L. J., Herrera, D., Barrett, D. J., Galford, G. L., Moran, C. J., & Soares-Filho, B. S. (2017). Mining drives extensive deforestation in the Brazilian Amazon. *Nature Communications*, *8*(1), 1013. https://doi.org/10.1038/s41467-017-00557-w

Swenson, J. J., Carter, C. E., Domec, J.-C., & Delgado, C. I. (2011). Gold Mining in the Peruvian Amazon: Global Prices, Deforestation, and Mercury Imports. *PLoS ONE*, *6*(4), e18875. https://doi.org/10.1371/journal.pone.0018875

Telmer, K., & Stapper, D. (2007). UNIDO PROJECT EG/GLO/01/G34 FINAL REPORT. *Final Report Evaluating and Monitoring Small Scale Gold Mining and Mercury Use: Building a Knowledge-Base with Satellite Imagery and Field Work 49*. https://www.unido.org/publications/ot/9656565/pdf

Terra-i. (2013, October 18). *Terra-i, An eye on habitat change—The Devastating Costs of the Rush for Gold in Madre de Dios, Peru*. http://www.terra-i.org/news/news/The-Devastating-Costs-of-the-Rush-for-Gold-in-Madre-de-Dios--Peru.html

Thanapol, P., Lavangnananda, K., Bouvry, P., Pinel, F., & Leprévost, F. (2020). Reducing Overfitting and Improving Generalization in Training Convolutional Neural Network (CNN) under Limited Sample Sizes in Image Recognition. *2020 - 5th International Conference on Information Technology (InCIT)*, 300–305. https://doi.org/10.1109/InCIT50588.2020.9310787

Toth, C., & Jóźków, G. (2016). Remote sensing platforms and sensors: A survey. *ISPRS Journal of Photogrammetry and Remote Sensing*, *115*, 22–36. https://doi.org/10.1016/j.isprsjprs.2015.10.004

USAID. (2020). *CASE STUDY: ARTISANAL AND SMALL-SCALE MINING IN MADRE DE DIOS, PERU*. https://www.planetgold.org/sites/default/files/2020-12/USAID.%202020.%20Case%20Study%20ASM%20and%20ASGM%20in%20Madre%20de%20Dios.pdf

USAID. (2020, January 28). *ISSUE BRIEF ARTISANAL & SMALL-SCALE MINING: USAID ACTIVITIES & APPROACHES*. https://tenuresecurity.org/wp-content/uploads/2020/01/USAID-ASM-Issue-Brief-Jan-2020.pdf

Wang, Y., Shang, L., Liu, Y., Sun, Z., Lu, Y., Shi, X., Wang, T., & Liu, Y. (2025). Precise building semantic segmentation in remote sensing images via MR-DeepLabv3+ network. *Scientific Reports*, *15*(1), 40100. https://doi.org/10.1038/s41598-025-23917-9

Wikipedia. (2026). Department of Madre de Dios. In *Wikipedia*. https://en.wikipedia.org/w/index.php?title=Department_of_Madre_de_Dios&oldid=1331060075#cite_note-1

Wikipedia. (2026a). Kayapo. In *Wikipedia*. https://en.wikipedia.org/w/index.php?title=Kayapo&oldid=1333723303#cite_note-posey-8

Wurm, M., Stark, T., Zhu, X. X., Weigand, M., & Taubenböck, H. (2019). Semantic segmentation of slums in satellite images using transfer learning on fully convolutional neural networks. *ISPRS Journal of Photogrammetry and Remote Sensing*, *150*, 59–69. https://doi.org/10.1016/j.isprsjprs.2019.02.006

Xu, S., Bu, Z., Zhang, Y., & Barnett, I. (2025). *A Hessian-informed hyperparameter optimization for differential learning rate* (arXiv:2501.06954). arXiv. https://doi.org/10.48550/arXiv.2501.06954

Xue, Z., & Zheng, Y. (2024). RB-Net: Rule-Based Neural Networks with Interpretable Models. *2024 Sixth International Conference on Next Generation Data-Driven Networks (NGDN)*, 64–68. https://doi.org/10.1109/NGDN61651.2024.10744176

Zhu, X. X., Tuia, D., Mou, L., Xia, G.-S., Zhang, L., Xu, F., & Fraundorfer, F. (2017). Deep Learning in Remote Sensing: A Comprehensive Review and List of Resources. *IEEE Geoscience and Remote Sensing Magazine*, *5*(4), 8–36. https://doi.org/10.1109/MGRS.2017.2762307

Masters
Program
in **Geospatial Technologies**

Supported by:
Education and Culture
ERASMUS MUNDUS